

at 5 kHz. The holding potential was clamped at -70 mV for recording of spontaneous postsynaptic current (sPSC). Liquid junctional potentials were not corrected. The Mini Analysis Program (Synptosoftware, Leonia, NJ) was used to analyze sPSC. Individual synaptic events were captured with threshold detectors using Mini Analysis software. All quantitative measurements were taken for 100 s. All data were plotted as a means \pm SEM.

Behavioral tests

The novel object recognition task was carried out as described elsewhere (Rampon et al., 2000). The mice were habituated for 3 days to an open field box ($50 \times 50 \times 40$ [height] cm). During the sample sessions, two novel objects (dice or marble) were placed into one end of the open field, and mice were allowed to explore these objects for 10 min. The time mice spent exploring each object was recorded. During the retention trials, performed 24 or 48 h later, a novel object (dice or marble) was placed together with the familiar object in the open field. The time mice spent exploring the two objects was recorded. A preference index (defined as the ratio of the amount of time mice spent exploring the novel object over the total time mice spent exploring both objects) was used as a measure of recognition memory. The social interaction test was previously described (Miyakawa et al., 2001). The Y-maze task was performed essentially as described previously (Mishima et al., 2004). Each arm was 40 cm long, 12 cm high, 3 cm wide at the bottom and 10 cm wide at the top. Each mouse was placed at the end of a fixed arm as a start arm (Fig. 7B), and was allowed to move freely through the maze during the 5-min test session. The sequence of arm entries was recorded manually. An alternation was defined as entry into all three arms on consecutive choices. The number of maximum alternations was then the total number of arms entered minus 2, and the percent alternation was calculated as (actual alternations/maximum alternations) \times 100. The arms were cleaned between animals.

Statistical analysis

Statistical comparisons of data were performed using an ANOVA followed by Fisher's probable least squares difference test for pairwise comparisons for behavioral studies and Western blotting experiments. Electrophysiological data were analyzed by using the Mann–Whitney U test. Results from CBF and histological experiments were analyzed by using Student's t test. $P < 0.05$ was considered to be statistically different.

Results

Constitutive constriction of cerebral arteries in vivo

We previously demonstrated that the lack of M_5 receptors nearly abolished ACh-mediated vasodilation of the basilar artery and cerebral arterioles (Yamada et al., 2001a). To examine whether $M_5R^{-/-}$ mice showed changes in arterial diameter in vivo, we employed time-of-flight (TOF) MRA which is sensitive to vessels with fast-flowing blood. TOF angiograms were obtained using a two-dimensional gradient-echo sequence (see Materials and methods). Maximum intensity projections (MIPs) were generated using standard software from the magnetic resonance system after zero-filling the raw data. The imaging parameters for MRA acquisition, including echo time (TE), repetition time (TR) and flip angle, had been optimized using $M_5R^{+/+}$ mice as a control (see Materials and

methods). We found that $M_5R^{-/-}$ mice (12-month-old mice) showed a significant decrease in diameter of the basilar artery (Figs. 1 and 2), indicative of a constitutive constriction of this vessel. Additionally, the lack of M_5 receptors led to a marked reduction of vascular diameter at the distal level of the arbor of the middle cerebral artery

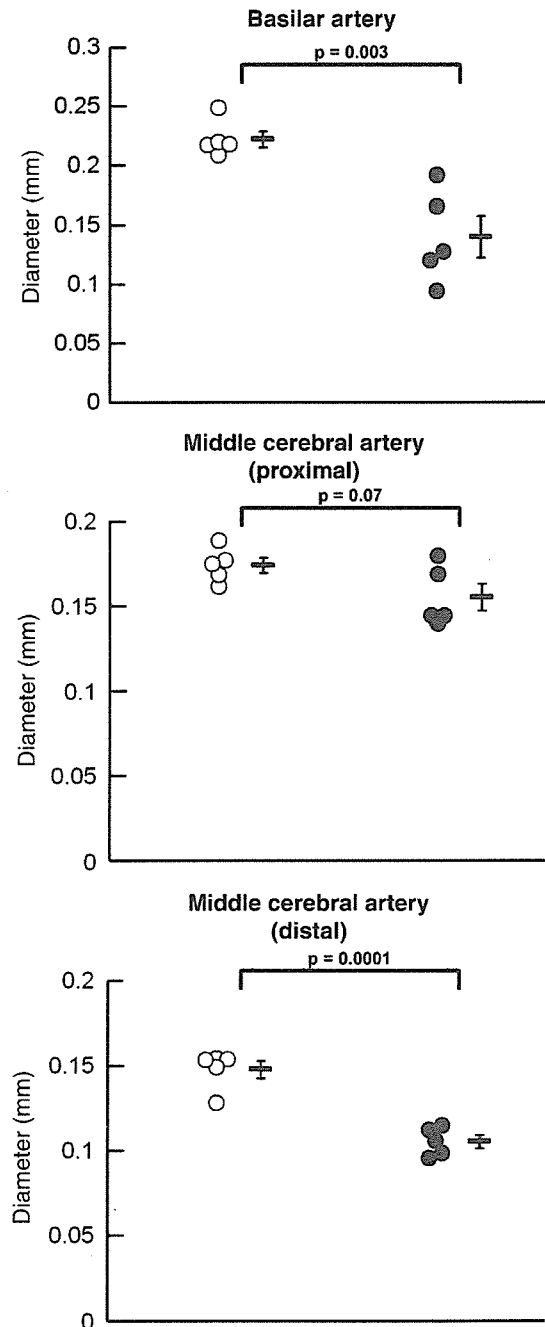


Fig. 2. Abnormalities in the cerebrovascular architecture of $M_5R^{-/-}$ mice studied by MRA. The diameter of the indicated cerebral blood vessels was measured from MIP images as described under Materials and methods. Arrows in Fig. 1 indicate the vascular regions (the basilar artery, the proximal level of the arbor of the MCA, and the distal level of the arbor of the MCA). Open circles, $M_5R^{+/+}$ mice; closed circles, $M_5R^{-/-}$ mice. Data represent means \pm SEM; $n = 5$ per group.

(MCA) in $M5R^{-/-}$ mice (Fig. 1). MRA also demonstrated a clear trend towards narrowing of vessels in proximal regions of the MCA (Figs. 1 and 2).

6-month-old $M5R^{-/-}$ mice showed significantly reduced diameter of basilar artery ($M5R^{+/+}$, 0.23 ± 0.02 mm; $M5R^{-/-}$, 0.20 ± 0.01 mm; mean \pm SEM; $M5R^{+/+}$, $n=8$; $M5R^{-/-}$, $n=7$; $p<0.05$) and distal MCA ($M5R^{+/+}$, 0.15 ± 0.01 mm; $M5R^{-/-}$, 0.12 ± 0.01 mm; mean \pm SEM; $M5R^{+/+}$, $n=8$; $M5R^{-/-}$, $n=7$; $p<0.05$). These data indicate that $M5R^{-/-}$ mice showed pronounced cerebrovascular deficits in vivo.

The brain volume of $M5R^{-/-}$ mice (12 months old) did not differ significantly from that of wild-type mice (Fig. 3), as calculated by T1 MRI. TUNEL staining did not reveal any signs of cell death in the whole brain of $M5R^{-/-}$ mice (data not shown).

Reduced CBF in $M5R^{-/-}$ mice

Angiograms of $M5R^{-/-}$ mice showed a substantial reduction of vascular diameter at the distal level of the arbor of the MCA (indicated by arrows in Fig. 1), which is located close to the surface of the cerebral cortex (see supplemental movie file 1, $M5R^{+/+}$ mice; supplemental movie file 2, $M5R^{-/-}$ mice). We therefore decided to measure CBF and the diameter of cerebral arterioles located on the cortical surface at the level of the peripheral branch of the MCA, using intravital microscopy through a cranial window in $M5R^{+/+}$ and

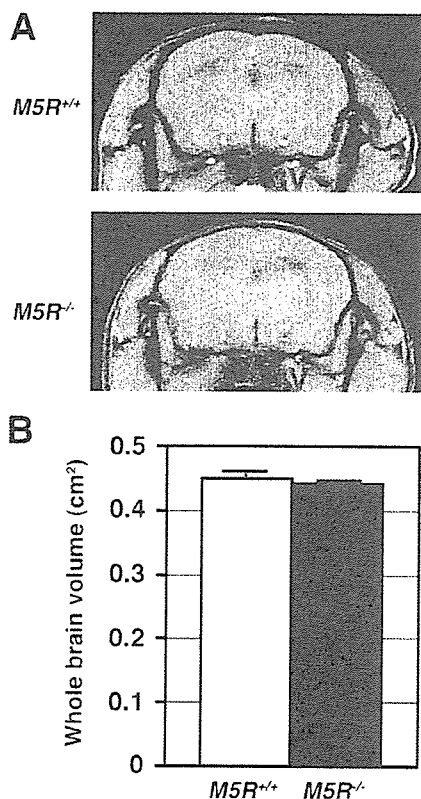


Fig. 3. Brain volume of $M5R^{-/-}$ and wild-type mice. (A) Morphometric investigation of living brains was conducted with 12-month-old mice by T1-weighted 2D gradient-echo MR scan. Arrowhead indicates 3V, third ventricle. (B) Volume of the whole brain was determined by using a PMOD software. 12-month-old $M5R^{-/-}$ mice did not show any difference from their wild-type littermates in brain volume ($P=0.20$; $n=5$ in each group).

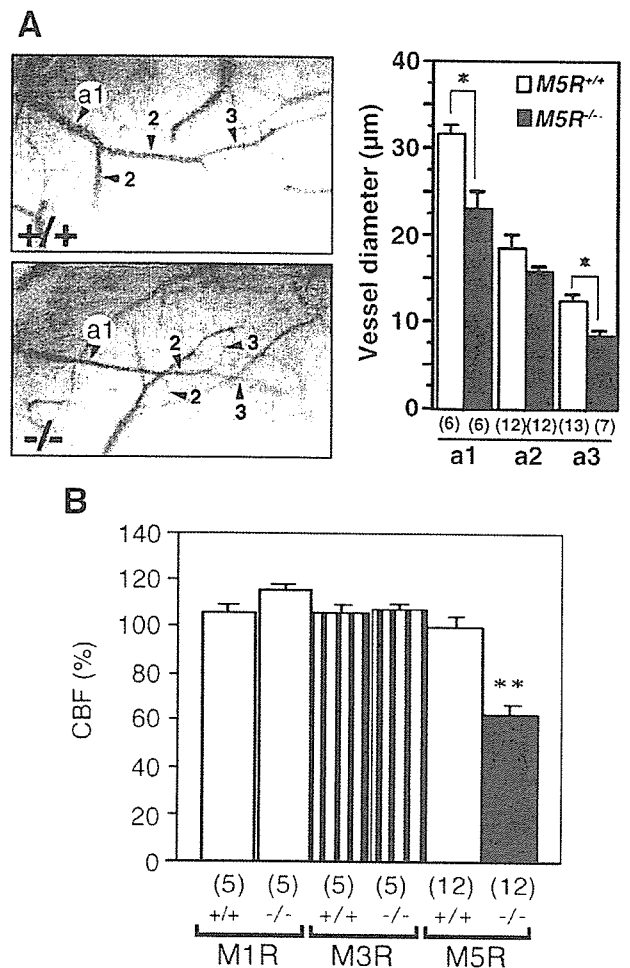


Fig. 4. Decreased diameter of cerebral arterioles and reduced CBF in $M5R^{-/-}$ mice. Unless stated otherwise, all studies were carried out with 3-month-old mice. (A) Photomicrographs of the middle cerebral artery and arterioles (MCA) of male $M5R^{-/-}$ and $M5R^{+/+}$ mice showing a reduction in blood vessel diameter in $M5R^{-/-}$ mice. (B) The diameter of different branches of the MCA (A1, A2, and A3 level; for classification scheme, see Refs. Horton, 1945; Fenton and Zweifach, 1981) was reduced in male $M5R^{-/-}$ mice. The bottom panels show resting blood flow through the MCA at the A1 level of (B) CBF in $M1$, $M3$ and $M5$ muscarinic receptor knockout mice (3 months old). The numbers given in parentheses underneath panels indicate the number of independent experiments (mice). Data are means \pm SEM; * $P<0.05$; ** $P<0.01$.

$M5R^{-/-}$ mice (3-month-old mice). All mice showed normal peripheral blood pressure (tail cuff method) ($M5R^{+/+}$, 111.6 ± 4.6 mm Hg; $M5R^{-/-}$, 111.8 ± 3.6 mm Hg; means \pm SEM; $n=8$ per group). The branches of the MCA were defined in the order from A1 to A3 (see Materials and methods). Under resting conditions, $M5R^{-/-}$ mice showed a small but significant reduction ($P<0.05$) in the diameter of middle cerebral arterioles, as compared with $M5R^{+/+}$ mice (Fig. 4A). Laser Doppler flowmeter measurements showed that $M5R^{-/-}$ mice showed significantly lower ($P<0.01$) CBF at the A1 branch in the resting state. This effect was not observed with $M1$ and $M3$ receptor muscarinic receptor knockout mice (the $M1$, $M3$, and $M5$ receptors are all coupled to G proteins of the G_q family) (Fig. 4B). We next quantified regional CBF in $M5R^{-/-}$ and $M5R^{+/+}$ mice (6-month-old mice) by using ^{14}C -labeled iodoanti-

pyrine autoradiography. $M5R^{-/-}$ mice displayed significantly reduced CBF ($P < 0.05$) in all cortical, hippocampal, and thalamic regions studied (Table 1). Such impairments in CBF were not observed in different regions of the midbrain (Table 1). These data indicate that the lack of $M5$ receptors leads to impaired CBF in higher brain regions. We note that $M5R^{-/-}$ mice showed an impaired autoregulation of CBF (data not shown).

Atrophy of cortical pyramidal neurons in $M5R^{-/-}$ mice

Cerebrovascular disturbances have been shown to be associated with structural changes of cortical pyramidal neurons including a reduced number of dendritic spines and thin dendrites (Langmeier et al., 1989; Schroder and Luhmann, 1997; Sakic et al., 2000; Hasbani et al., 2001). We therefore investigated whether cortical pyramidal neurons (layer V) from $M5R^{-/-}$ mice showed similar deficits. Golgi staining studies revealed that cortical pyramidal neurons from $M5R^{-/-}$ mice (6 months old) showed clear signs of atrophy of the basal-dendritic tree and apical dendrites (Fig. 5A) (number of spines per 10 μ m length of dendritic segment: $M5R^{+/+}$, 8.91 ± 0.10 ; $M5R^{-/-}$, 7.02 ± 0.15 ; means \pm SEM; $P < 0.05$; $n = 40$ dendritic segments from 3 animals per group). A likely scenario is that the cerebrovascular deficiencies displayed by the $M5R^{-/-}$ mice are

Table 1
Resting cerebral blood flow (CBF) measured by autoradiography in male $M5R^{-/-}$ and $M5R^{+/+}$ mice

Regions	CBF, ml/100 g per min		% Difference
	$M5R^{+/+}$	$M5R^{-/-}$	
<i>Cerebral cortex</i>			
Frontal cortex	136.7 \pm 4.0	117.5 \pm 6.4 *	-14
Somatosensory cortex	142.3 \pm 3.1	123.2 \pm 4.0 *	-13
Parietal cortex	149.1 \pm 3.1	129.5 \pm 6.0 *	-13
Temporal cortex	156.2 \pm 5.4	126.7 \pm 6.4 *	-19
Occipital cortex	136.3 \pm 3.3	117.3 \pm 3.5 *	-14
<i>Basal ganglia</i>			
Caudate-putamen	128.3 \pm 4.0	105.0 \pm 3.5 *	-18
Globus pallidus	90.7 \pm 2.9	86.3 \pm 3.1	-5
Amygdala	103.2 \pm 4.0	88.5 \pm 1.8 *	-14
<i>Hippocampus</i>			
CA1	90.2 \pm 3.0	76.0 \pm 2.7 *	-16
CA3	90.7 \pm 3.7	78.7 \pm 2.1 *	-13
Dentate gyrus	91.0 \pm 3.0	78.8 \pm 2.7 *	-13
<i>Thalamic nuclei</i>			
Anterior	154.2 \pm 4.3	133.3 \pm 5.4 *	-14
Reticular	149.7 \pm 3.9	127.8 \pm 5.2 *	-15
Ventrobasal	147.2 \pm 7.7	122.7 \pm 4.1 *	-17
Ventromedial	152.8 \pm 4.9	124.7 \pm 3.7 *	-18
Intralaminar	148.0 \pm 3.3	116.5 \pm 4.1 *	-21
Hypothalamus	99.2 \pm 3.9	83.5 \pm 3.6 *	-16
<i>Midbrain</i>			
Substantia nigra	92.7 \pm 3.3	86.0 \pm 2.6	-7
Superior colliculus	148.7 \pm 3.1	143.3 \pm 3.0	-4
Inferior colliculus	209.3 \pm 4.7	196.5 \pm 3.7	-6

Local CBF was measured by quantitative autoradiography using 14 C-labeled iodoantipyrine (IAP) as a tracer. All values are means \pm SEM; $n = 6$ per group (6-month-old mice).

* $P < 0.05$ vs. $M5R^{-/-}$.

responsible for the altered morphology of cortical pyramidal neurons.

We also analyzed the expression of several key neuronal receptor proteins by using Western blot analysis. Specifically, we examined the expression levels of the NR1 [*N*-methyl-D-aspartate (NMDA) receptor subunit], GluR1 (AMPA receptor subunit), and GluR5 (kainate receptor subunit) glutamate receptor subunits. $M5R^{-/-}$ mice (6 months old) showed reduced expression levels of NR1 and GluR5 receptors in cerebral cortex and hippocampus (Fig. 5B) as compared to $M5R^{+/+}$ mice, whereas GluR1 expression levels in hippocampus remained unaffected (Fig. 5B). We observed significantly reduced NR1 expression levels in cortex and hippocampus from 2-month-old but not from 1-month-old $M5R^{-/-}$ mice (data not shown).

Reduced neuronal activity and LTP in hippocampal preparations from $M5R^{-/-}$ mice

Golgi staining studies revealed that $M5R^{-/-}$ mice (6 months old) also showed significant morphological deficits of the CA2 and CA3 hippocampal pyramidal neurons and the granule cells of the dentate gyrus. The neurons from $M5R^{-/-}$ mice exhibited a significantly reduced number of dendritic spines in all regions of the hippocampus (CA2, CA3, and dentate gyrus; Fig. 6A), except for the CA1 region. To evaluate the functional activity of CA3 pyramidal neurons from $M5R^{+/+}$ and $M5R^{-/-}$ mice, we carried out whole-cell patch-clamp recordings using freshly prepared hippocampal slices. The CA3 pyramidal neurons were selected for electrophysiological experiments because they form an essential link in the hippocampal synaptic circuit implicated in learning and memory (O'Keefe and Nadel, 1978; Barnes, 1988; Morris et al., 1990; Seress and Ribak, 1995). TUNEL staining did not reveal any signs of cell death in the hippocampus (CA1–CA3 and dentate gyrus) of $M5R^{-/-}$ mice (data not shown). In CA3 pyramidal neurons from $M5R^{-/-}$ mice (6 months old), the frequency of the spontaneous postsynaptic current (sPSC) was significantly reduced ($P < 0.05$; Fig. 6B). However, sPSC amplitudes did not differ significantly between $M5R^{+/+}$ and $M5R^{-/-}$ mice (data not shown).

We also found that the lack of $M5$ receptors was associated with a reduction in the number of dendritic spines of dentate gyrus neurons (Fig. 6A). To examine whether this deficit was associated with changes in neuronal plasticity, we studied long-term potentiation (LTP) at the mossy fiber-CA3 synapse using hippocampal slices from $M5R^{+/+}$ and $M5R^{-/-}$ mice (6-month-old males). The lack of $M5$ receptors had no significant effect on the input–output relationship between presynaptic fiber volleys and the field excitatory postsynaptic potential (fEPSP) (data not shown). High-frequency tetanic stimulation (TS) reliably produced LTP of excitatory transmission at the mossy fiber-CA3 synapse from $M5R^{+/+}$ mice (Fig. 6C). Strikingly, LTP was significantly reduced ($P = 0.004$) in preparations from $M5R^{-/-}$ mice (Fig. 6C). Moreover, paired-pulse stimulation experiments suggested that neurotransmitter release from mossy fiber terminals was also impaired in $M5R^{-/-}$ mice (Fig. 6D). These data indicate that the lack of $M5$ receptors leads to severe impairments of hippocampal neuronal circuits.

Impairment of hippocampus-dependent memory in $M5R^{-/-}$ mice

The hippocampus plays a key role in the formation of many forms of memory including recognition memory (O'Keefe and Nadel, 1978; Barnes, 1988; Morris et al., 1990; Seress and Ribak,

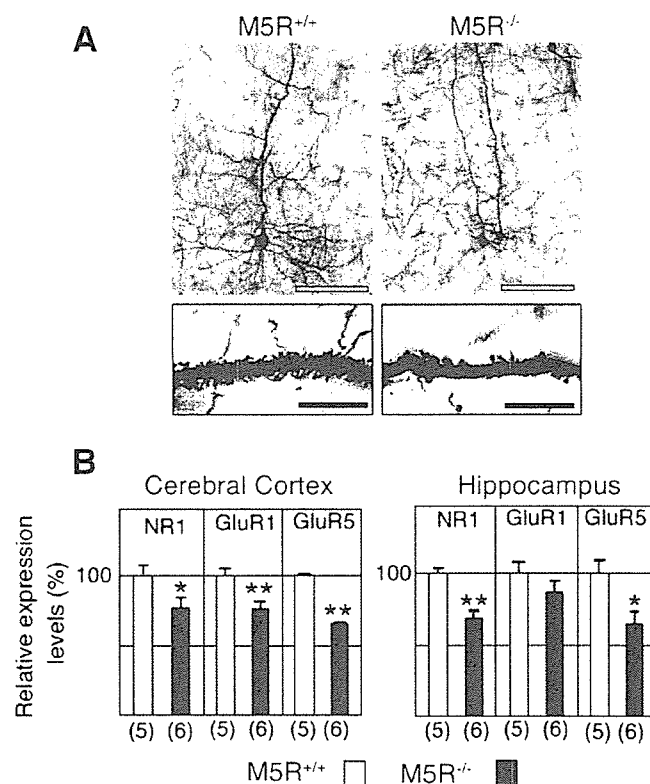


Fig. 5. Altered morphology of cortical pyramidal neurons and reduced glutamate receptor expression levels in cortex and hippocampus from $M5R^{-/-}$ mice. (A) Morphologic changes revealed by Golgi staining of cortical pyramidal neurons (layer V) from $M5R^{-/-}$ mice. Golgi staining studies revealed that cortical pyramidal neurons from male $M5R^{-/-}$ mice (6 months old) showed clear signs of atrophy of the basal-dendritic tree and apical dendrites. White scale bars in upper panels, 50 μm ; black scale bars in lower panels, 10 μm . (B) Relative expression levels, determined by Western blot analysis, of cortical and hippocampal glutamate receptor subunits in 6-month-old male $M5R^{-/-}$ and $M5R^{+/+}$ (=100%) mice. The numbers given in parentheses underneath panels indicate the number of independent experiments (mice). Data represent means \pm SEM; * P <0.05; ** P <0.001.

1995). We therefore examined whether recognition memory was altered in congenic $M5R^{-/-}$ mice, using the novel object recognition test (Rampon et al., 2000). We used this test since previous work had shown that atrophy of CA1–CA3 hippocampal pyramidal neurons leads to cognitive deficits in spatial and nonspatial memory (McEwen, 2002; Conrad et al., 2003). We found that the locomotor activity did not differ significantly between the two groups (6-month-old mice; cm traveled/10 min: $M5R^{+/+}$, 1813 ± 228 ; $M5R^{-/-}$, 1775 ± 310 ; means \pm SEM; $n=10$ per group). Two identical objects were placed at one end of an open field, and the amount of time that mice spent exploring the two objects was recorded (Fig. 7A). During the initial sample trial, the total exploration time was not significantly different among the two genotypes ($M5R^{+/+}$, 21.8 ± 3.9 s; $M5R^{-/-}$, 17.9 ± 3.7 s; means \pm SEM; $n=10$ per group). Moreover, no significant exploratory preference for one of the two objects was found in either group (Fig. 7C). These observations indicated that the absence of M_5 receptors had no effect on motivation and curiosity in exploring new objects. During test trials (recognition/retention testing), carried out 24 and 48 h after the initial training, one of the two objects was replaced with a novel object. A preference index (the ratio of the amount of time mice spent exploring the novel object over the total time mice spent exploring both objects) was used as a measure of recognition memory. $M5R^{+/+}$ mice showed a significant preference for exploring the novel object in the recognition/retention trials (P <0.05; Fig. 7D). In contrast, $M5R^{-/-}$ mice did not show any preference for the

novel object (Fig. 7D). In a social interaction test, the two groups did not show any significant differences in the number of social contacts (interactions/5 min: $M5R^{+/+}$, 37.3 ± 2.2 ; $M5R^{-/-}$, 34.0 ± 2.5 ; means \pm SEM; $n=10$ per group; $P=0.33$), excluding the possibility that $M5R^{-/-}$ mice are simply more anxious than $M5R^{+/+}$ mice.

To explore potential differences in hippocampal working memory between $M5R^{+/+}$ and $M5R^{-/-}$ mice, we used the Y-maze spontaneous alternation spatial working test (see Fig. 7B for a diagram of this test). Spontaneous alternation is often used as a measure of exploratory behavior and spatial working memory, which are known to be related to hippocampal memory function (Conrad et al., 2003; Cavalli et al., 1997; Mishima et al., 2004). In the Y-maze task, male $M5R^{-/-}$ mice (6 months old) showed impaired spontaneous alternation performance (P <0.05; Fig. 7E).

Discussion

The activation of cholinergic neurons has been shown to play an important role in the regulation of cerebral vascular resistance, relaxation and contraction of blood vessels, and regional blood flow (Faraci and Sigmund, 1999; Hotta et al., 2002; Sato et al., 2004). ACh, by activating muscarinic receptors expressed by vascular endothelial cells, is a powerful dilator of cerebral vascular beds (Faraci and Sigmund, 1999). Recent studies suggest that M_5 receptors expressed by vascular endothelial cells play a key role in mediating ACh-induced relaxation of cerebral arteries and arterioles

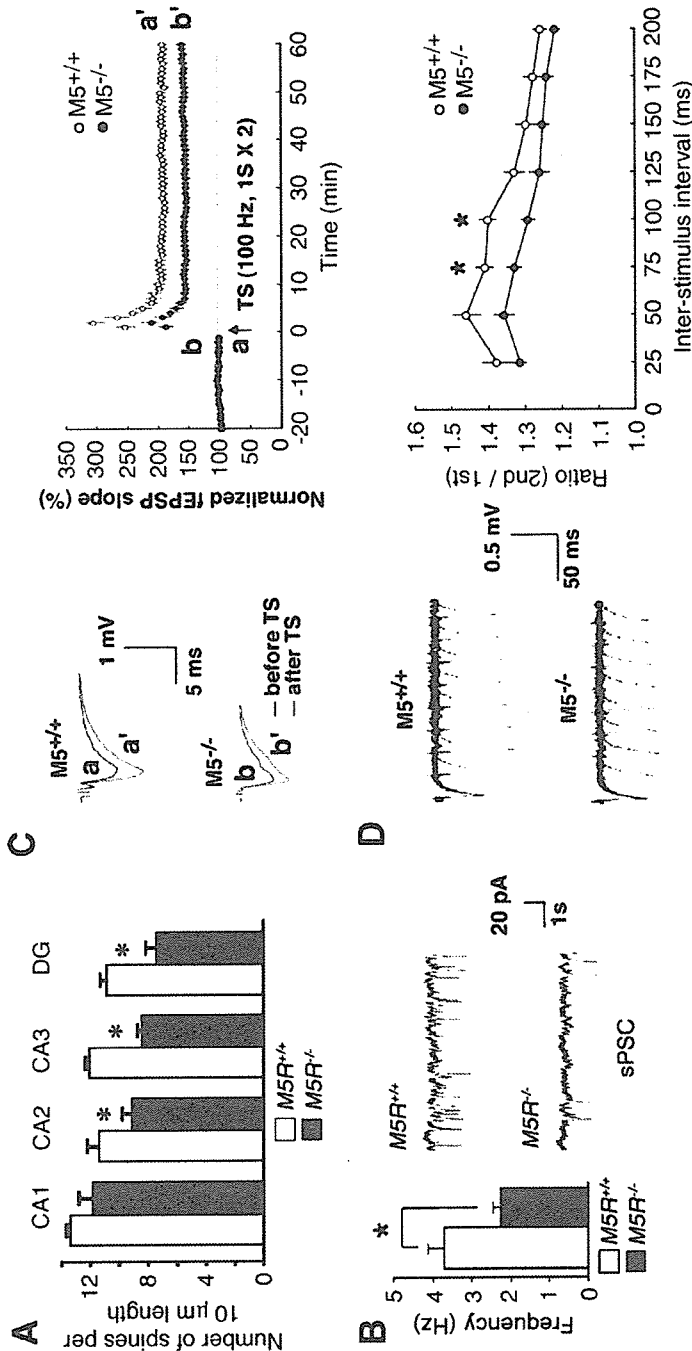


Fig. 6. Altered morphology and reduced neuronal activity in the hippocampus of *M5R^{-/-}* mice. All studies were carried out with 6-month-old male *M5R^{-/-}* and *M5R^{+/+}* mice. (A) Golgi staining showing a significant reduction in the number of dendritic spines in CA2 and CA3 pyramidal and dentate gyrus (DG) neurons from *M5R^{-/-}* mice. Data are expressed as number of spines per 10 μm from secondary dendrites extending from primary dendrites within the molecular layer. Data are given as means ± SEM; * *P* < 0.05; *n* = 20–30 dendritic segments from 3 animals per group. (B) Spontaneous neuronal activity of CA3 pyramidal neurons is reduced in *M5R^{-/-}* mice. The frequency of the spontaneous postsynaptic current (sPSC) was recorded from CA3 pyramidal neurons of *M5R^{-/-}* and *M5R^{+/+}* mice. The sPSC was measured at a holding potential of -70 mV. The frequency of sPSCs was significantly decreased (*P* < 0.05) in *M5R^{-/-}* mice (*M5R^{-/-}*, 2.25 ± 0.22 Hz, *n* = 20 cells from 5 mice; *M5R^{+/+}*, 3.72 ± 0.41 Hz, *n* = 17 cells from 5 mice). The right panels show representative sPSC traces. (C) Impaired hippocampal function and plasticity in *M5R^{-/-}* mice. The left panel shows representative sample traces of field excitatory postsynaptic potentials (fEPSPs) before (blue line; a) and 60 min after high-frequency tetanic stimulation (TS) (red line; a'). Long-term potentiation (LTP) at mossy fiber-CA3 pyramidal cell synapses was impaired in *M5R^{-/-}* mice. The LTP amplitude was significantly reduced in *M5R^{-/-}* mice (*M5R^{-/-}*, 192.4 ± 7.1%, *n* = 12 slices from 5 mice; *M5R^{+/+}*, 161.3 ± 7.6%, *n* = 12 slices from 5 mice, measured 60 min after TS; *P* = 0.0047). (D) Short-term synaptic plasticity in *M5R^{-/-}* and *M5R^{+/+}* mice. Paired-pulse facilitation (PPF) at the CA3 pyramidal cell synapse is impaired in *M5R^{-/-}* mice (*M5R^{-/-}* mice, 1.33 ± 0.02, *P* < 0.05) and 100 ms (*M5R^{-/-}* mice, 1.40 ± 0.02; *M5R^{+/+}* mice, 1.29 ± 0.02, *P* < 0.05). (E) The magnitude of PPF in mutant mice was significantly reduced at stimulus intervals of 75 ms (*M5R^{-/-}* mice, 1.41 ± 0.02; *M5R^{+/+}* mice, 1.33 ± 0.02, *P* < 0.05) and 100 ms (*M5R^{-/-}* mice, 1.40 ± 0.02; *M5R^{+/+}* mice, 1.29 ± 0.02, *P* < 0.05).

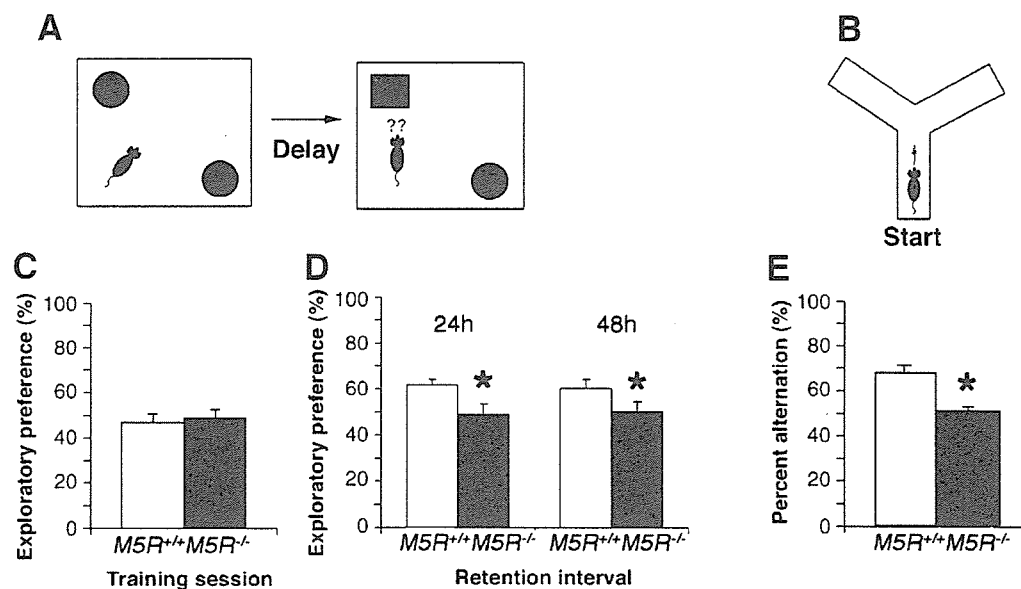


Fig. 7. Impaired performance of $M5R^{-/-}$ mice in an object recognition memory test and a Y-maze working memory task. All studies were carried out with 6-month-old $M5R^{-/-}$ and $M5R^{+/+}$ mice. (A) Diagram of the object recognition memory task. (B) Diagram of the Y-maze spontaneous alternation spatial working memory test. (C) In the novel object recognition memory task, the period of time mice spent exploring two identical objects in a same sample trial (training session) was examined in male $M5R^{-/-}$ and $M5R^{+/+}$ mice. The lack of M_5 receptors had no significant effect on exploratory preference in the sample trial. (D) Retention testing in the novel object recognition memory task of male $M5R^{-/-}$ and $M5R^{+/+}$ mice. For retention testing, carried out 24 and 48 h after the training session, one of the two objects was replaced with a novel object. A preference index, the ratio of the amount of time mice spent exploring the novel object over the total time mice spent exploring both objects, was used as a measure of recognition memory. Note that only male $M5R^{-/-}$ mice failed to show a significant increase in the amount of time spent exploring the new object. Data are given as means \pm SEM; $n = 10$ per group; * $P < 0.05$. (E) Performance of male $M5R^{-/-}$ and $M5R^{+/+}$ mice in the Y-maze spontaneous alternation task. Note that only male $M5R^{-/-}$ mice showed a performance deficit in this test. Data are given as means \pm SEM; $M5R^{-/-}$, $n = 19$ mice; $M5R^{+/+}$, $n = 10$ –13 mice; * $P < 0.05$.

(Hamel, 2004; Yamada et al., 2001a; Wang et al., 1994). Cortical microvessels are deficient in cholinergic neurogenic control in Alzheimer's disease (Tong and Hamel, 1999) and central cholinergic stimulation with cholinesterase inhibitors, such as physostigmine and donepezil, can reverse the decrease in cortical blood flow observed in Alzheimer's disease (Geaney et al., 1990; Nakano et al., 2001), suggesting that deficits in cortical cholinergic vasodilation may play a role in the pathophysiology of this disorder. In the present study, we therefore tested the hypothesis that the permanent lack of M_5 receptors may cause cerebrovascular insufficiencies, which may potentially lead to impaired neuronal dysfunction and cognitive deficits.

We demonstrated that the absence of cerebrovascular M_5 receptors was associated with pronounced reductions in CBF in all cortical, hippocampal, and thalamic regions studied. In vivo MRA techniques revealed that $M5R^{-/-}$ mice showed a pronounced constitutive constriction of cerebral arteries (basilar artery, MCA), suggesting that tonic activation of M_5 receptors plays a key role in maintaining proper cerebrovascular function.

Expression of the M_5 receptor gene in mammalian cell lines has shown that the encoded receptor protein is functional and efficiently couples to G proteins of the G_q family, similar to the M_1 and M_3 receptor subtypes (Wess, 2004; Wess et al., 2003). Previously we showed that M_5 receptors play role in mediating ACh-induced relaxation of cerebral but not of peripheral blood vessels (Yamada et al., 2001a). We also reported that ACh-induced dilation of peripheral blood vessels is mediated, at least in part, by M_3 receptors (Khurana et al., 2005). To further study the subtype selectivity of muscarinic receptor-dependent vasodilation

mechanisms, we carried out CBF measurements with M_1 , M_3 and M_5 receptor-deficient mice using laser Doppler flowmetry (CBF measurements were taken at the A1 level of the MCA). These studies showed that only M_5 receptor-deficient mice showed significantly reduced CBF in MCA, suggesting that acetylcholine-dependent activation of M_5 receptors plays an important role in regulating cerebral circulation.

Impaired autoregulation of CBF is known to be associated with the deterioration of the cerebral microcirculation (Kobari et al., 1994; Jones et al., 1999; Matsushita et al., 1994; Tong and Hamel, 1999). Like the $M5R^{-/-}$ mice, the APP transgenic mice showed impaired autoregulation of CBF and markedly attenuated cerebrovascular responses to ACh (Niwa et al., 2002; Iadecola, 2004). Impaired autoregulation of CBF is also commonly observed in the elderly human population (Melamed et al., 1980; Shaw et al., 1984; Choi et al., 1998; Jagust, 2000; Rapoport, 2000; Lee et al., 2003).

Several recent studies suggest that morphological changes in dendritic arbors, spines, and synapses are associated with learning and memory (Rampon et al., 2000; McEwen, 2002; Conrad et al., 2003; Geinisman et al., 1986; Swaab, 2003; Poirazi and Mel, 2001). We found that sPSC was significantly reduced in CA3 pyramidal neurons in $M5R^{-/-}$ mice. The CA3 pyramidal cells are thought to store new episodic information as it arrives via a number of specialized preprocessing stages from associated areas of the cortex (Vinogradova, 2001). The dentate granule cell/mossy fiber system is important during learning, as it helps produce a new pattern of firing in the CA3 cells during each learning episode. We found that LTP was significantly reduced at the mossy fiber-CA3 synapse in $M5R^{-/-}$

mice, suggesting that the functional connectivity of hippocampal circuits is impaired in the absence of M₅ receptors. In agreement with these findings, the *M5R*^{-/-} mice showed significant deficits in hippocampus-dependent spatial and nonspatial memory tasks. Several lines of evidence suggest that decreased CBF may lead to reduced synthesis of proteins involved in learning and memory, resulting in changes in neuronal plasticity and cognitive impairments (Iadecola, 2004; Mies et al., 1991; Hossmann, 1994). It has been demonstrated that mossy fiber-LTP is impaired in GluR6-deficient mice (Contractor et al., 2001) or GluR5 antagonist LY 382884 (Bortolotto et al., 1999; Lauri et al., 2001). Consistent with this finding, *M5R*^{-/-} mice showed a significant reduction in the density of various cortical and hippocampal glutamate receptor subunits known to be involved in cognitive processes. These findings raise the possibility that the impairments in hippocampal LTP and cognitive functions displayed by the *M5R*^{-/-} mice are a consequence of reduced CBF caused by the absence of cerebrovascular M₅ receptors.

At this point, we cannot completely rule out the possibility that the deficits observed with the *M5R*^{-/-} mice are due to the lack of M₅ receptors during the development of the nervous system, rather than being caused by the direct absence of M₅ receptors in the brain. Furthermore, we observed significantly reduced NR1 expression levels in cortex and hippocampus from 2-month-old but not from 1-month-old *M5R*^{-/-} mice. However, we did not observe any signs of cell death by TUNEL staining and brain volume was normal in 12-month-old *M5R*^{-/-} mice. We are planning to address this issue in future studies by using conditional *M5R*^{-/-} mice.

One of the hallmarks of Alzheimer's disease is the gradual loss of the cholinergic innervation of higher brain areas (Coyle et al., 1983; Bartus, 2000). Our data therefore suggest the possibility that at least some of the functional and behavioral deficits associated with Alzheimer's disease are caused by impaired signaling through cerebrovascular M₅ receptors. The development of selective M₅ receptor agonists may therefore lead to novel therapeutic agents useful in the symptomatic treatment of Alzheimer's disease and related disorders.

Acknowledgments

We thank Drs. F. Faraci and M. Ogawa, K. Takeuchi for their helpful discussions and H. Morishita, H. Kishida, Y. Matsuba, and S. Yamamoto for their expert technical assistance. M.Y. and K.S. are recipients of a Grant-in-aid for Scientific Research (B) from The Ministry of Education Culture, Sports, and Technology (MEXT) of Japan. T.N. is a recipient of a RIKEN Special Postdoctoral Researchers Program 13-091 and Daiwa Securities Health Foundation.

Appendix A. Supplementary Data

Supplementary data associated with this article can be found, in the online version, at doi:10.1016/j.nbd.2006.07.010.

References

- Barnes, C.A., 1988. Spatial learning and memory processes: the search for their neurobiological mechanisms in the rat. *Trends Neurosci.* 11, 163–169.
- Bartus, R.T., 2000. On neurodegenerative diseases, models, and treatment strategies: lessons learned and lessons forgotten a generation following the cholinergic hypothesis. *Exp. Neurol.* 163, 495–529.
- Bortolotto, Z.A., Clarke, V.R., Delany, C.M., Parry, M.C., Smolders, I., Vignes, M., Ho, K.H., Miu, P., Brinton, B.T., Fantaske, R., Ogden, A., Gates, M., Ornstein, P.L., Lodge, D., Bleakman, D., Collingridge, G.L., 1999. Kainate receptors are involved in synaptic plasticity. *Nature* 402, 297–301.
- Cavalli, A., Lattion, A.L., Hummler, E., Nenniger, M., Pedrazzini, T., Aubert, J.F., Michel, M.C., Yang, M., Lembo, G., Vecchione, C., Mostardini, M., Schmidt, A., Beermann, F., Cotecchia, S., 1997. Decreased blood pressure response in mice deficient of the alpha1b-adrenergic receptor. *Proc. Natl. Acad. Sci. U. S. A.* 94, 11589–11594.
- Choi, J.Y., Morris, J.C., Hsu, C.Y., 1998. Aging and cerebrovascular disease. *Neurol. Clin.* 16, 687–711.
- Conrad, C.D., Grote, K.A., Hobbs, R.J., Ferayorni, A., 2003. Sex differences in spatial and nonspatial Y-maze performance after chronic stress. *Neurobiol. Learn. Mem.* 79, 32–40.
- Contractor, A., Swanson, G., Heinemann, S.F., 2001. Kainate receptors are involved in short- and long-term plasticity at mossy fiber synapses in the hippocampus. *Neuron* 29, 209–216.
- Coyle, J.T., Price, D.L., DeLong, M.R., 1983. Alzheimer's disease: a disorder of cortical cholinergic innervation. *Science* 219, 1184–1190.
- Davies, P., Maloney, A.J., 1976. Selective loss of central cholinergic neurons in Alzheimer's disease. *Lancet* 2, 1403.
- Dunphy, M.J., Goble, D.D., Smith, D.J., 1990. Nitrate analysis by capillary gas chromatography. *Anal. Biochem.* 184, 381–387.
- Faraci, F.M., Sigmund, C.D., 1999. Vascular biology in genetically altered mice: smaller vessels, bigger insight. *Circ. Res.* 85, 1214–1225.
- Fenton, B.M., Zweifach, B.W., 1981. Microcirculatory model relating geometrical variation to change in pressure and flow rate. *Ann. Biomed. Eng.* 9, 303–321.
- Fisahn, A., Yamada, M., Duttaroy, A., Gan, J.W., Deng, C.X., McBain, C.J., Wess, J., 2002. Muscarinic induction of hippocampal gamma oscillations requires coupling of the M1 receptor to two mixed cation currents. *Neuron* 33, 615–624.
- Geaney, D., Soper, N., Shepstone, B.J., Cowen, P.J., 1990. Effect of central cholinergic stimulation on regional cerebral blood flow in Alzheimer disease. *Lancet* 335, 1484–1487.
- Geinisman, Y., de Toledo-Morrell, L., Morrell, F., 1986. Loss of perforated synapses in the dentate gyrus: morphological substrate of memory deficit in aged rats. *Proc. Natl. Acad. Sci. U. S. A.* 83, 3027–3031.
- Gomi, S., Gotoh, F., Ishihara, N., Tanaka, K., Ishikawa, Y., Takashima, S., Mihara, B., 1991. Effects of lesioning of the substantia innominata on autoregulation of local cerebral blood flow in rats. *J. Cereb. Blood Flow Metab.* 11, 66–71.
- Hamel, E., 2004. Cholinergic modulation of the cortical microvascular bed. *Prog. Brain Res.* 145, 171–178.
- Hasbani, M.J., Schlieff, M.L., Fisher, D.A., Goldberg, M.P., 2001. Dendritic spines lost during glutamate receptor activation reemerge at original sites of synaptic contact. *J. Neurosci.* 21, 2393–2403.
- Higuchi, M., Iwata, N., Matsuba, Y., Sato, K., Sasamoto, K., Saido, T.C., 2005. ¹⁹F- and ¹H-MRI detection of amyloid-beta plaques in vivo. *Nat. Neurosci.* 8, 527–533.
- Horton, R.E., 1945. Erosional development of streams and their drainage basins: hydrophysical approach to quantitative morphology. *Geol. Soc. Am. Bull.* 56, 275–370.
- Hossmann, K.A., 1994. Viability thresholds and the penumbra of focal ischemia. *Ann. Neurol.* 36, 557–565.
- Hotta, H., Uchida, S., Kagitani, F., 2002. Effects of stimulating the nucleus basalis of Meynert on blood flow and delayed neuronal death following transient ischemia in the rat cerebral cortex. *Jpn. J. Physiol.* 52, 383–393.
- Iadecola, C., 2003. Cerebrovascular effects of amyloid-beta peptides: mechanisms and implications for Alzheimer's dementia. *Cell. Mol. Neurobiol.* 23, 681–689.

- Iadecola, C., 2004. Neurovascular regulation in the normal brain and in Alzheimer's disease. *Nat. Rev., Neurosci.* 5, 347–360.
- Jagust, W.J., 2000. Neuroimaging in dementia. *Neurol. Clin.* 18, 885–902.
- Jay, T.M., Lucignani, G., Crane, A.M., Jehle, J., Sokoloff, L., 1988. Measurement of local cerebral blood flow with [¹⁴C]iodoantipyrine in the mouse. *J. Cereb. Blood Flow Metab.* 8, 121–129.
- Jones, S.C., Radinsky, C.R., Furlan, A.J., Chyatte, D., Perez-Trepichio, A.D., 1999. Cortical NOS inhibition raises the lower limit of cerebral blood flow-arterial pressure autoregulation. *Am. J. Physiol.* 276, H1253–H1262.
- Kamiya, H., Umeda, K., Ozawa, S., Manabe, T., 2002. Presynaptic Ca²⁺ entry is unchanged during hippocampal mossy fiber long-term potentiation. *J. Neurosci.* 22, 10524–10528.
- Khurana, S., Yamada, M., Wess, J., Kennedy, R.H., Raufman, J.P., 2005. Deoxycholytaurine-induced vasodilation of rodent aorta is nitric oxide- and muscarinic M₃ receptor-dependent. *Eur. J. Pharmacol.* 517, 103–110.
- Kobari, M., Fukuuchi, Y., Tomita, M., Tanahashi, N., Takeda, H., 1994. Role of nitric oxide in regulation of cerebral microvascular tone and autoregulation of cerebral blood flow in cats. *Brain Res.* 667, 255–262.
- Langmeier, M., Pokorny, J., Mares, J., Trojan, S., 1989. Changes of the neuronal structure produced by prolonged hypobaric hypoxia in infant rats. *Biomed. Biochim. Acta* 48, S204–S207.
- Lauri, S.E., Bortolotto, Z.A., Bleakman, D., Ornstein, P.L., Lodge, D., Isaac, J.T., Collingridge, G.L., 2001. A critical role of a facilitatory presynaptic kainate receptor in mossy fiber LTP. *Neuron* 32, 697–709.
- Lee, B.C., Mintun, M., Buckner, R.L., Morris, J.C., 2003. Imaging of Alzheimer's disease. *J. Neuroimaging* 13, 199–214.
- Levey, A.I., 1996. Muscarinic acetylcholine receptor expression in memory circuits: implications for treatment of Alzheimer disease. *Proc. Natl. Acad. Sci. U. S. A.* 93, 13541–13546.
- Matsushita, K., Kuriyama, Y., Nagatsuka, K., Nakamura, M., Sawada, T., Omae, T., 1994. Periventricular white matter lucency and cerebral blood flow autoregulation in hypertensive patients. *Hypertension* 23, 565–568.
- McEwen, B.S., 2002. Sex, stress and the hippocampus: allostasis, allostatic load and the aging process. *Neurobiol. Aging* 23, 921–939.
- Melamed, E., Lavy, S., Bentin, S., Cooper, G., Rinot, Y., 1980. Reduction in regional cerebral blood flow during normal aging in man. *Stroke* 11, 31–35.
- Mies, G., Ishimaru, S., Xie, Y., Seo, K., Hossmann, K.A., 1991. Ischemic thresholds of cerebral protein synthesis and energy state following middle cerebral artery occlusion in rat. *J. Cereb. Blood Flow Metab.* 11, 753–761.
- Mishima, K., Tanoue, A., Tsuda, M., Hasebe, N., Fukue, Y., Egashira, N., Takano, Y., Kamiya, H.O., Tsujimoto, G., Iwasaki, K., Fujiwara, M., 2004. Characteristics of behavioral abnormalities in α_{1D} -adrenoceptors deficient mice. *Behav. Brain Res.* 152, 365–373.
- Miyakawa, T., Yamada, M., Duttaroy, A., Wess, J., 2001. Hyperactivity and intact hippocampus-dependent learning in mice lacking the M₁ muscarinic acetylcholine receptor. *J. Neurosci.* 21, 5239–5250.
- Morris, R.G., Schenk, F., Tweedie, F., Jarrard, L.E., 1990. Ibotenate lesions of hippocampus and/or subiculum: dissociating components of allocentric spatial learning. *Eur. J. Neurosci.* 2, 1016–1028.
- Nakano, S., Asada, T., Matsuda, H., Uno, M., Takasaki, M., 2001. Donepezil hydrochloride preserves regional cerebral blood flow in patients with Alzheimer's disease. *J. Nucl. Med.* 42, 1441–1445.
- Niwa, K., Kazama, K., Younkin, L., Younkin, S.G., Carlson, G.A., Iadecola, C., 2002. Cerebrovascular autoregulation is profoundly impaired in mice overexpressing amyloid precursor protein. *Am. J. Physiol.: Heart Circ. Physiol.* 283, H315–H323.
- Noguchi, T., Sasaki, Y., Seki, J., Giddings, J.C., Yamamoto, J., 1999. Effects of voluntary exercise and L-arginine on thrombogenesis and microcirculation in stroke-prone spontaneously hypertensive rats. *Clin. Exp. Pharmacol. Physiol.* 26, 330–335.
- O'Keefe, J., Nadel, L., 1978. *The Hippocampus as a Cognitive Map*. Oxford Univ. Press.
- Panel, E., Yasutake, K., Fujita, S.C., Ishiguro, K., 2001. Inhibition of protein phosphatase 2A overrides tau protein kinase I/glycogen synthase kinase 3 beta and cyclin-dependent kinase 5 inhibition and results in tau hyperphosphorylation in the hippocampus of starved mouse. *J. Biol. Chem.* 276, 34298–34306.
- Poirazi, P., Mel, B.W., 2001. Impact of active dendrites and structural plasticity on the memory capacity of neural tissue. *Neuron* 29, 779–796.
- Rampon, C., Tang, Y.P., Goodhouse, J., Shimizu, E., Kyin, M., Tsien, J.Z., 2000. Enrichment induces structural changes and recovery from nonspatial memory deficits in CA1 NMDAR1-knockout mice. *Nat. Neurosci.* 3, 238–344.
- Rapoport, S.I., 2000. Functional brain imaging to identify affected subjects genetically at risk for Alzheimer's disease. *Proc. Natl. Acad. Sci. U. S. A.* 97, 5696–5698.
- Sakic, B., Kolb, B., Whishaw, I.Q., Gorny, G., Szechtman, H., Denburg, J.A., 2000. Immunosuppression prevents neuronal atrophy in lupus-prone mice: evidence for brain damage induced by autoimmune disease? *J. Neuroimmunol.* 111, 93–101.
- Sakurada, O., Kennedy, C., Jehle, J., Brown, J.D., Carbin, G.L., Sokoloff, L., 1978. Measurement of local cerebral blood flow with iodo [¹⁴C] antipyrine. *Am. J. Physiol.* 234, H59–H66.
- Sato, A., Sato, Y., Uchida, S., 2004. Activation of the intracerebral cholinergic nerve fibers originating in the basal forebrain increases regional cerebral blood flow in the rat's cortex and hippocampus. *Neurosci. Lett.* 361, 90–93.
- Schroder, R., Luhmann, H.J., 1997. Morphology, electrophysiology and pathophysiology of supragranular neurons in rat primary somatosensory cortex. *Eur. J. Neurosci.* 9, 163–176.
- Seki, K., Kudoh, M., Shibuki, K., 2001. Sequence dependence of post-tetanic potentiation after sequential heterosynaptic stimulation in the rat auditory cortex. *J. Physiol.* 533, 503–518.
- Seress, L., Ribak, C.E., 1995. Postnatal development of CA3 pyramidal neurons and their afferents in the Ammon's horn of rhesus monkeys. *Hippocampus* 5, 217–231.
- Shaw, T.G., Mortel, K.F., Meyer, J.S., Rogers, R.L., Hardenberg, J., Cutaja, M.M., 1984. Cerebral blood flow changes in benign aging and cerebrovascular disease. *Neurology* 34, 855–862.
- Swaab, D.F., 2003. Reactivation of atrophic neurons in Alzheimer's disease. *Neurol. Res.* 25, 652–660.
- Tayebati, S.K., Di Tullio, M.A., Tomassoni, D., Amenta, F., 2003. Localization of the m5 muscarinic cholinergic receptor in rat circle of Willis and pial arteries. *Neuroscience* 122, 205–211.
- Tong, X.K., Hamel, E., 1999. Regional cholinergic denervation of cortical microvessels and nitric oxide synthase-containing neurons in Alzheimer's disease. *Neuroscience* 92, 163–175.
- Vinogradova, O.S., 2001. Hippocampus as comparator: role of the two input and two output systems of the hippocampus in selection and registration of information. *Hippocampus* 11, 578–598.
- Wang, S.Z., Zhu, S.Z., El-Fakahany, E.E., 1994. Efficient coupling of m5 muscarinic acetylcholine receptors to activation of nitric oxide synthase. *J. Pharmacol. Exp. Ther.* 268, 552–557.
- Wess, J., 2004. Muscarinic acetylcholine receptor knockout mice: novel phenotypes and clinical implications. *Annu. Rev. Pharmacol. Toxicol.* 44, 423–450.
- Wess, J., Duttaroy, A., Zhang, W., Gomeza, J., Cui, Y., Miyakawa, T., Bymaster, F.P., McKinzie, L., Felder, C.C., Lamping, K.G., Faraci, F.M., Deng, C., Yamada, M., 2003. M₁–M₅ muscarinic receptor knockout mice as novel tools to study the physiological roles of the muscarinic cholinergic system. *Recept. Channels* 9, 279–290.
- Yamada, M., Lamping, K.G., Duttaroy, A., Zhang, W., Cui, Y., Bymaster, F.P., McKinzie, D.L., Felder, C.C., Deng, C.X., Faraci, F.M., Wess, J., 2001a. Cholinergic dilation of cerebral blood vessels is abolished in M5 muscarinic acetylcholine receptor knockout mice. *Proc. Natl. Acad. Sci. U. S. A.* 98, 14096–14101.
- Yamada, M., Miyakawa, T., Duttaroy, A., Yamanaka, A., Moriguchi, T., Makita, R., Ogawa, M., Chou, C.J., Xia, B., Crawley, J.N., Felder, C.C., Deng, C., Wess, J., 2001b. Mice lacking the M₃ muscarinic acetylcholine receptor are hypophagic and lean. *Nature* 410, 207–212.

The players on the γ -secretase team

Akihiko Takashima, Masafumi Shimojo & Benjamin Wolozin

A β generation requires γ -secretase activity. Inhibition of γ -secretase may now be easier due to the recent identification of the four proteins that make up the γ -secretase complex.

In Alzheimer disease, accumulation of amyloid- β (A β), a cleavage product of amyloid precursor protein (APP), impairs memory and leads to neuronal death. The toxicity associated with accumulation of A β suggests that activation of endoproteolytic enzymes capable of preventing generation of A β might provide a realistic target for pharmacotherapy of Alzheimer disease. On the other hand, cleavage of APP by β - and γ -secretase generates A β peptides. β -secretase, which initiates cleavage of APP, cuts the protein at the N terminus and has been successfully cloned. γ -secretase is the second enzyme that cleaves APP, and full understanding of its mechanism of action has long been lacking. Reconstitution of γ -secretase activity illuminates the interaction between the various protein components of the γ -secretase complex that leads to formation of A β ¹.

Either presenilin-1 (PS1) or presenilin-2 (PS2) makes up the first component of the γ -secretase complex. Mutations in the genes that encode PS1 and PS2 cause a subset of early-onset, familial Alzheimer disease. Presenilin mutations probably act upstream of APP or tau to cause Alzheimer disease pathology, including deposition of A β and accumulation of hyperphosphorylated tau. For example, mutant presenilins have been shown to increase formation of the longer A β species, A β ₄₂. This species is important for Alzheimer disease pathology because it accelerates deposition of A β , which presumably precipitates early-onset Alzheimer disease. Thus, disease-related mutations in presenilin are considered to shift cleavage of APP by γ -secretase toward increased A β ₄₂ production².

Both presenilin-deficient cell lines and presenilin-deficient mice do not generate A β but do produce larger APP fragments which are the substrate for γ -secretase³. In addition, dominant negative PS1 mutants inhibit A β production⁴ and a γ -secretase inhibitor that recognizes a transitional state of γ -secretase binds to a PS1

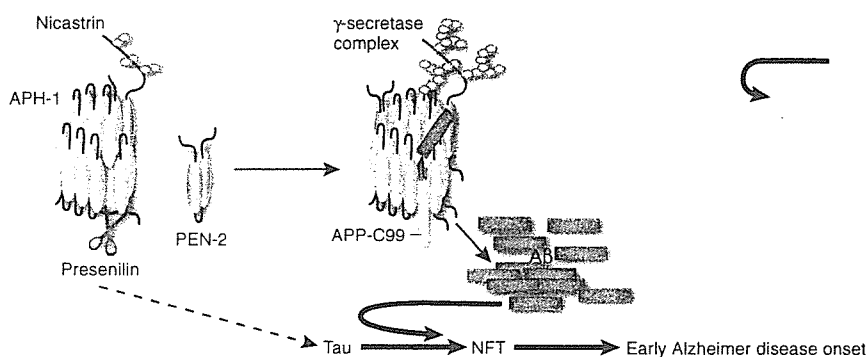


Figure 1 Presenilin, APh1 and nicastrin first form a stable complex. After association with PEN-2 and cleavage of presenilin, the complex becomes active γ -secretase, and clips its substrate, APP-C99, to generate A β species. An aggregated form of A β is neurotoxic and induces tau hyperphosphorylation, leading to formation of neurofibrillary tangles (NFTs) and neuronal death. On the other hand, independent of this cascade, reducing the levels of components in the γ -secretase complex induces hyperphosphorylation of tau. Mutant presenilin may therefore be independently involved in formation of both NFTs and A β . PS1 mutations may directly accelerate the rate of NFT formation in aging, and further accelerate NFT formation and neurodegeneration by increasing the rate of A β aggregation. Eventually, the accumulation of A β and NFTs precipitated by the PS1 mutation causes the cognitive dysfunction associated with early-onset Alzheimer disease.

fragment⁵. These results provide strong support for the hypothesis that presenilin directly participates in γ -secretase activity. Yet, the emerging story has not vanquished all questions about the role of presenilin in γ -secretase activity, as overexpression of presenilin does not increase production of A β .

In fact, presenilin is a part of a large, high-molecular-weight complex with γ -secretase activity. Nicastrin, the product of a recently cloned gene, is a component of this γ -secretase complex⁶. Overexpressing the two genes together, however, does not ramp up γ -secretase activity⁷. Instead, other proteins are required.

Studies of Notch signaling in *C. elegans*, which depends on γ -secretase activity⁸, provide additional information about γ -secretase activity. Aph-1 and PEN-2 are two transmembrane proteins that are expressed upstream of release of the Notch intracellular domain^{9,10}. When these proteins are knocked down, γ -secretase activity decreases, which suggests that these two proteins may also be involved in γ -secretase activity^{9,11}.

The results described above indicate that four proteins (presenilin, nicastrin, Aph-1 and PEN-2) are required for γ -secretase activity, but none of them generate γ -secretase activity on

their own; an increase in activity is only possible when the four proteins are overexpressed together^{1,11} (Fig. 1). Thus, it is clear that these four proteins are essential components needed for γ -secretase activity.

With this report the outstanding question of presenilin's role in γ -secretase activity is revealed, but a bigger question now looms: how do presenilin mutations lead to Alzheimer disease? A PS1 mutation has been implicated in frontotemporal dementia¹², a disease associated with tau pathology. In addition, mutant PS1 knock-in mice exhibit an acceleration of tau pathology¹³. Therefore, presenilin mutations might have a bigger role in mediating aggregation of tau into neurofibrillary tangles (NFTs) than was previously considered. Alzheimer disease may result from a sequential process that begins with deposition of A β but has a more widely distributed and complex pathology. The classic pathological hallmarks of Alzheimer disease, A β plaques and tau-containing NFTs, may be independent developments that interact with each other. PS1 mutations might aggravate this interaction, which would trigger the early onset of Alzheimer disease (Fig. 1). The involvement of γ -secretase components in hyperphosphorylation of tau supports the hypothesis that mutations in PS1

Akihiko Takashima and Masafumi Shimojo are in the Laboratory for Alzheimer's Disease, RIKEN, Brain Science Institute, 2-1 Hirotsawa, Wako-si, Saitama 351-0198, Japan, and Benjamin Wolozin is in the Department of Pharmacology, Boston University School of Medicine, Boston, Massachusetts 02118-2536, USA.
E-mail: kenneth@brain.riken.go.jp

Kim Caesar



contribute to formation of NFTs¹⁴. Thus, the γ -secretase complex might be involved in protease activity, but may also act independently to induce tau pathology (Fig. 1). Elucidating the functions of the γ -secretase complex could illuminate as much about the development of tau-associated pathology in Alzheimer disease as it does about the development of amyloid pathol-

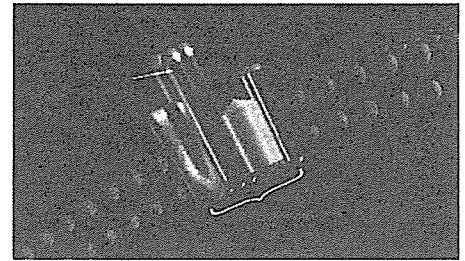
ogy, and ultimately reveal the primary causes of this devastating disease.

1. Edbauer, D. *et al. Nat. Cell Biol.* **5**, 486–488 (2003).
2. Scheuner, D. *et al. Nat. Med.* **2**, 864–870 (1996).
3. De Strooper, B. *et al. Nature* **391**, 387–390 (1998).
4. Wolfe, M.S. *et al. Nature* **398**, 513–517 (1999).
5. Li, Y.M. *et al. Nature* **405**, 689–694 (2000).
6. Yu, G. *et al. Nature* **407**, 48–54 (2000).
7. Chung, H.M. *et al. Nat. Cell Biol.* **3**, 1129–1132 (2001).
8. De Strooper, B. *et al. Nature* **398**, 518–522 (1999).
9. Francis, R. *et al. Dev. Cell* **3**, 85–97 (2002).
10. Goutte, C. *et al. Proc. Natl. Acad. Sci. USA* **99**, 775–779 (2002).
11. Takasugi, N. *et al. Nature* **422**, 438–441 (2003).
12. Dermaut, B. *et al. Trends Genet.* **21**, 664–672 (2005).
13. Tanemura, K. *et al. J. Biol. Chem.* **281**, 5037–5041 (2006).
14. Doglio, L.E. *et al. Neuron* **50**, 359–375 (2006).

The author's perspective

Although the project design, involving a reporter gene assay for γ -secretase activity in an organism that lacks this activity, was conceptually clear-cut and straightforward from the beginning, it took six years of work until we identified the proteins responsible for γ -secretase activity. The project began by using our reporter gene assay in yeast to screen a human gene library for the γ -secretase gene and continued with directly testing the presenilin gene alone or in combination with the nicastrin gene for γ -secretase activity. All these experiments were unsuccessful. In retrospect it was clear why. It takes four proteins to reconstitute γ -secretase.

Having established the identity of γ -secretase as a complex of the subunits presenilin, nicastrin, Aph-1 and Pen-2, we are now concentrating on the function of the individual proteins in the complex. Apart from the role of presenilin as the catalytic subunit and the recent finding that nicastrin serves as a γ -secretase substrate receptor, the functional role of the other complex components is still unclear. Recently, we found that several γ -secretase complexes coexist in human cells. We are currently trying to determine whether these individual complexes have distinct functions.




Courtesy of the NIA

Harald Steiner, Ludwig-Maximilians-University

Recent papers on Alzheimer disease identified by leaders in the field as notable advances^a

Reference	Percent ^b
Klunk, W.E. <i>et al.</i> Imaging brain amyloid in Alzheimer's disease with Pittsburgh Compound-B. <i>Ann. Neurol.</i> 55 , 306–319 (2004)	29
Lesne, S. <i>et al.</i> A specific amyloid- β protein assembly in the brain impairs memory. <i>Nature</i> 440 , 352–357 (2006)	29
SantaCruz, K. <i>et al.</i> Tau suppression in a neurodegenerative mouse model improves memory function. <i>Science</i> 309 , 476–481 (2005)	26
Rovelet-Lecrux, A. <i>et al.</i> APP locus duplication causes autosomal dominant early-onset Alzheimer disease with cerebral amyloid angiopathy. <i>Nat. Genet.</i> 38 , 24–26 (2006)	24
Gilman, S. <i>et al.</i> Clinical effects of A β immunization (AN1792) in patients with AD in an interrupted trial. <i>Neurology</i> 64 , 1553–1562 (2005)	21
Oddo, S. <i>et al.</i> Triple-transgenic model of Alzheimer's disease with plaques and tangles: intracellular A β and synaptic dysfunction. <i>Neuron</i> 39 , 409–421 (2003)	21
Edbauer, D. <i>et al.</i> Reconstitution of γ -secretase activity. <i>Nat. Cell Biol.</i> 5 , 486–488 (2003)	21
Cirrito, J.R. <i>et al.</i> Synaptic activity regulates interstitial fluid amyloid- β levels <i>in vivo</i> . <i>Neuron</i> 48 , 913–922 (2005)	21
Kayed, R. <i>et al.</i> Common structure of soluble amyloid oligomers implies common mechanism of pathogenesis. <i>Science</i> 300 , 486–489 (2003)	18
Lazarov, O. <i>et al.</i> Environmental enrichment reduces A β levels and amyloid deposition in transgenic mice. <i>Cell</i> 120 , 701–713 (2005)	18
Shah, S. <i>et al.</i> Nicastrin functions as a γ -secretase-substrate receptor. <i>Cell</i> 122 , 435–447 (2005)	15
Cleary, J.P. <i>et al.</i> Natural oligomers of the amyloid- β protein specifically disrupt cognitive function. <i>Nat. Neurosci.</i> 8 , 79–84 (2005)	15
Takasugi, N. <i>et al.</i> The role of presenilin cofactors in the γ -secretase complex. <i>Nature</i> 422 , 438–441 (2003)	12
Snyder, E.M. <i>et al.</i> Regulation of NMDA receptor trafficking by amyloid- β . <i>Nat. Neurosci.</i> 8 , 1051–1058 (2005)	12
Nicoll, J.A. <i>et al.</i> Neuropathology of human Alzheimer disease after immunization with amyloid- β peptide: a case report. <i>Nat. Med.</i> 9 , 448–452 (2005)	12
Kamenetz, F. <i>et al.</i> APP processing and synaptic function. <i>Neuron</i> 37 , 925–937 (2003)	12
Hutter-Paier, B. <i>et al.</i> The ACAT inhibitor CP-113,818 markedly reduces amyloid pathology in a mouse model of Alzheimer's disease. <i>Neuron</i> 44 , 227–238 (2004)	12
Eriksen, J.L. <i>et al.</i> NSAIDs and enantiomers of flurbiprofen target γ -secretase and lower A β 42 <i>in vivo</i> . <i>J. Clin. Invest.</i> 112 , 440–449 (2003)	12

^aWe asked a panel of 34 prominent researchers interested in Alzheimer disease to identify what they considered to be the key papers in the field published since 2003, excluding papers from their own lab. This issue features News and Views on the first eight papers from the list. The rest are accompanied by a Research Highlight. ^bPercent of experts that selected each paper.



IOS Press is an International STM publisher
of books and journals in major scientific areas

You are a user of:
Rikagaku Kenkyujo

[Log out](#)

- [Publications](#)
- [About](#)
- [Search](#)
- [Browse](#)
- [Account](#)
- [Shopping Cart](#)
- [Order History](#)
- [Activate Access](#)
- [Register](#)
- [Services](#)
- [Favorites](#)
- [Alerting](#)
- [ActiveSearch](#)
- [Support](#)
- [Contact Us](#)
- [Downloads](#)
- [Linking](#)

Article

[Back To: Main](#) [o Publication](#) [o Issue](#)



Journal of Alzheimer's Disease

Issue: Volume 9, Supplement 3 / 2006

Pages: 309 - 317

URL: [Linking Options](#)

GSK-3 is essential in the pathogenesis of Alzheimer's disease

Akihiko Takashima ^{A1}

^{A1} Laboratory for Alzheimer's Disease, Riken, Brain Science Institute, 2-1 Hirosawa, Wako-si, Saitama 351-0198, Japan. E-mail: kenneth@brain.riken.go.jp

Abstract:

Glycogen synthase kinase-3 (GSK-3) is a pivotal molecule in the development of Alzheimer's disease (AD). GSK-3 β is involved in the formation of paired helical filament (PHF)-tau, which is an integral component of the neurofibrillary tangle (NFT) deposits that disrupt neuronal function, and a marker of neurodegeneration in AD. GSK-3 β has exactly the same oligonucleotide sequence as tau-protein kinase I (TPKI), which was first purified from the microtubule fraction of bovine brain. Initially, we discovered that GSK-3 β was involved in amyloid- β (A β)-induced neuronal death in rat hippocampal cultures. In the present review, we discuss our initial in vitro results and additional investigations showing that A β activates GSK-3 β through impairment of phosphatidylinositol-3 (PI3)/Akt signaling; that A β -activated GSK-3 β induces hyperphosphorylation of tau, NFT formation, neuronal death, and synaptic loss (all found in the AD brain); that GSK-3 β can induce memory deficits in vivo; and that inhibition of GSK-3 α (an isoform of GSK-3 β) reduces A β production. These combined results strongly suggest that GSK-3 activation is a critical step in brain aging and the cascade of detrimental events in AD, preceding both the NFT and neuronal death pathways. Therefore, therapeutics targeted to inhibiting GSK-3 may be beneficial in the treatment of this devastating disease.

Keywords:

GSK-3 β , NFT, A β , AD, tauopathy

Full Text Access

Full Text Secured

The full text of this article is secured to subscribers. To gain access, you may:

- [Subscribe to this publication.](#)

[Subscribe](#)

- [Add this item to your shopping cart for purchase later.](#)

[Add to Shopping Cart](#)

- [Purchase this item now.](#)

[Purchase Item Now](#)

- [Log in to verify access.](#)

[Log In](#)

Please note:

By using this site you agree to the terms of our copyright for pay-per-view access.

Increased levels of granular tau oligomers: An early sign of brain aging and Alzheimer's disease

Sumihiro Maeda^{a,b}, Naruhiko Sahara^a, Yuko Saito^c, Shigeo Murayama^c,
Atsushi Ikai^b, Akihiko Takashima^{a,*}

^aLab for Alzheimer's Disease, Brain Science Institute, RIKEN, 2-1 Hirosawa, Wako, Saitama 351-0198, Japan

^bDepartment of Life Science, Graduate School of Bioscience and Biotechnology, Tokyo Institute of Technology, 4259 Nagatsuda, Midori-Ku, Yokohama, Kanagawa 226-8501, Japan

^cDepartment of Neuropathology, Tokyo Metropolitan Institute of Gerontology, 35-2 Sakaecho, Itabashi-ku, Tokyo 173-0015, Japan

Received 2 November 2005; accepted 25 November 2005

Available online 6 January 2006

Abstract

Development of neurofibrillary tangles (NFTs) is a pathological hallmark in various neurodegenerative disorders including Alzheimer's disease (AD). Recently, we identified a granular tau oligomer having a pre-filamentous structure. To determine the role of this oligomer in NFT formation, we quantified the amount of granular tau oligomer in 21 frontal cortex samples, each displaying varying degrees of Braak-staged NFT pathology. Here we report that granular tau oligomer levels in frontal cortex were significantly increased, even in brains displaying Braak-stage I neuropathology, a stage at which clinical symptoms of AD and NFTs in frontal cortex are believed to be absent. This suggests that increases in granular tau oligomer levels occur before NFTs form and before individuals manifest clinical symptoms of AD. Increased granular tau oligomer levels, therefore, may lead to NFT formation in frontal cortex, eventually leading to the development of AD. Thus, increases in granular tau oligomer levels may represent a very early sign of NFT formation and AD.

© 2005 Elsevier Ireland Ltd and the Japan Neuroscience Society. All rights reserved.

Keywords: Alzheimer's disease (AD); Tau; Atomic force microscopy (AFM); Granular tau oligomer; Braak stage; Brain aging

1. Introduction

Tau, a microtubule-associated protein, can aggregate into filamentous polymer forms (von Bergen et al., 2005). Bundled tau filaments that deposit in cells are called neurofibrillary tangles (NFTs), which commonly form in the brain during normal aging and in Alzheimer's disease (AD). In AD, NFTs and neuronal cell loss typically coincide within the same brain regions (Gomez-Isla et al., 1997). The progressively expanding anatomical distribution of NFTs reflects progressive brain dysfunction in disease, suggesting that NFT formation and neuronal cell loss may share a common mechanism (Ihara, 2001). The recent finding that patients with frontotemporal dementia and parkinsonism linked to chromosome 17 (FTDP-17) harbor tau mutations (Reed et al., 2001), strongly suggests

that tau dysfunction itself can cause neurodegeneration. Indeed, the overexpression of tau in various animal models has been shown to induce neurodegeneration (Lee et al., 2001; Tanemura et al., 2001, 2002; Tatebayashi et al., 2002). However, others have observed that neuronal cell loss occurs disproportionately to the number of NFTs in AD (Gomez-Isla et al., 1997). Conversely, others have reported neuronal loss in the absence of NFTs in a tau-overexpressing *Drosophila* model (Wittmann et al., 2001), suggesting that the events that lead from tau accumulation to neurodegeneration may not involve filament formation. Recently, (Santacruz et al., 2005) reported that reducing tau overexpression in mutant tau transgenic mice decreased neuronal cell loss even though filaments continued to form, suggesting that filament formation may not be the underlying cause of neuronal cell loss. Therefore, tau may be involved in neuronal dysfunction even before NFTs are formed.

Using an in vitro tau aggregation system, we identified a granular-shaped pre-filamentous form of tau – the granular tau oligomer – composed of about 40 tau molecules (Maeda et al.,

* Corresponding author.

E-mail address: kenneth@brain.riken.go.jp (A. Takashima).

unpublished data). We found that increasing the concentration of granular tau oligomers *in vitro* causes them to convert into filaments. The breakdown of PHF into granular tau structure by continuous AFM imaging has also been observed, indicating that granular tau oligomer composes of filament *in vivo*. In the present study, to understand the relationship between the levels of granular tau oligomer and the progression of AD, we quantified the amount of granular tau oligomer in various brain samples, each histopathologically confirmed to display different Braak stages (Braak and Braak, 1991). We then compared the amounts of granular tau oligomer in each Braak-staged sample using atomic force microscopy (AFM). We found increased levels of granular tau oligomer in brain samples at Braak stage I, a stage indicative of pre-symptomatic AD. Granular tau oligomers were detected even in samples at Braak stage 0.

2. Materials and methods

2.1. Subjects

Frozen frontal cortex samples from 21 subjects, including 5 patients with AD (Murayama and Saito, 2004), were obtained from the Tokyo Metropolitan Institute of Gerontology (TMIG) (Saito et al., 2004). The brains from TMIG were staged histopathologically according to the Braak staging system (Braak and Braak, 1991).

2.2. Antibodies

Anti-paired helical filament antibody, PHF-1, was a kind gift from Dr. P. Davies (Albert Einstein College of Medicine, USA). Anti-tau antibody, JM, was raised against full-length recombinant tau (Takashima et al., 1998). Anti-tau antibody, Tau-c, was raised against tau c-terminus polypeptide (amino acids 422–438, according to the longest human tau isoform).

2.3. Purification of granular tau oligomers

Human brain samples (~12 g) were homogenized with three volumes of a buffer containing 10 mM Tris (pH 7.4), 800 mM NaCl, 1 mM EGTA, 10% sucrose, and protease inhibitors, and centrifuged at $27,000 \times g$ for 20 min at 4 °C. CHAPS (Dojindo, Kumamoto, Japan) was added to the supernatant to a final concentration of 1% (w/v), then loaded into an immunoaffinity column (2 ml bed volume) containing anti-tau antibody JM. The column was washed with at least 400 ml of buffer containing 10 mM Tris (pH 7.4), 800 mM NaCl, 1 mM EGTA, and 1% CHAPS. After confirming that no aggregates remained in the wash solution, the column was eluted with 5 ml of 3M KSCN (Jicha et al., 1999). After exchanging the above buffer to a buffer containing 10 mM Tris (pH 7.4), 800 mM NaCl, and 1 mM EGTA with a NAP-10 column (Amersham Biosciences), we added *N*-lauroylsarcosine (Nacalai tesque, Kyoto, Japan) until achieving a final concentration of 1% (wt./vol.). After 2 h of incubation, 1 ml of sample was layered onto a sucrose step gradient (50, 40, 30, and 20% sucrose) and centrifuged for 2 h at 50 K rpm in a MLS50 rotor (Beckman Coulter) using an Optima MAX-E ultracentrifuge (Beckman Coulter) at 23 °C. We separated the samples into 1 ml fractions, from top to bottom (fractions 1–5), to eliminate contamination from lower fractions. We washed the bottom of tubes with buffer and saved the wash solution as fraction 6. We previously isolated granular tau oligomer from fraction 3 derived from either *in vitro* aggregated tau or human brain samples (Maeda et al., unpublished data). In the present study, we also found that the granular tau oligomer localized to fraction 3.

2.4. Western blot analysis

Granular tau oligomer fractions were concentrated by adding trichloroacetic acid to the fractions and setting the mixtures on ice for 2 h. The mixtures were

then centrifuged at $20,000 \times g$ at 4 °C, and supernatants were removed and dried in a SpeedVac Concentrator (SAVANT). Loading buffer was added to the dried granular tau oligomers, and this mixture was subjected to SDS-PAGE and subsequent immunoblotting with anti-tau antibody Tau-c.

Sarcosyl-insoluble fractions were prepared by solubilizing homogenized brain tissue (see above) in 1% sarcosyl for 2 h at 25 °C, then centrifuging at 50 K rpm in a TLA 55 rotor (Beckman Coulter) for 20 min. After removing the supernatant, loading buffer was added to the pellet, and the insoluble tau was subjected to SDS-PAGE and immunoblotting with PHF-1 antibody. Immunoreactivities were quantified with the software program Image Gauge (Fujifilm).

2.5. Atomic force microscopy

Samples were dropped onto freshly cleaved mica and left in place for 30 min prior to AFM assessment. After washing the mica with water, we examined the tau-containing samples in solution using a Nanoscope IIIa (Digital Instruments, Santa Barbara, CA, USA) set at tapping mode (Hansma et al., 1995). OMCL-TR400PSA (Olympus, Japan) was used as a cantilever. The resonant frequency was about 9 kHz.

We examined four different areas ($2 \mu\text{m} \times 2 \mu\text{m}$ each) of the mica surface covered with granular aggregates. These areas were analyzed with NIH-image 1.63 and summations of four different areas were demonstrated.

2.6. Statistical analysis

The significant difference between each Braak staging was tested with Mann–Whitney test. Data were analyzed with Prism 4 for Macintosh (Graphpad, San Diego, CA, USA).

3. Results

3.1. Purification of granular tau oligomers

We purified granular tau oligomers from human frontal cortices (Table 1) pathologically classified according to the Braak staging system (Braak and Braak, 1991) and examined the oligomers using AFM. Fig. 1 shows representative AFM images of cortex samples from a Braak-stage 0 brain (non-AD) and a Braak-stage V brain (AD). Although we detected granular tau oligomers in both of these samples, the number of oligomers in the Braak-stage V sample was much greater than that in the Braak-stage 0 sample. The size of granular tau oligomers ranged from 5 to 50 nm. The peak of granular tau oligomer was around 20 nm in diameter, which is similar with *in vitro* generated granular tau oligomer. And granular tau oligomers derived from *in vivo* and *in vitro* were recovered into same fraction in sucrose centrifugation, indicating the similar sedimentation coefficient between them. PHF-1 immunoreactivity and similar bands pattern with PHF-tau on immunoblotting (Fig. 2b and c, Maeda et al., unpublished data) suggested the hyperphosphorylation in granular tau oligomer.

3.2. Accumulation of granular tau oligomers during early stages of NFT formation

We quantified the number of granular tau oligomers in Braak-staged cortex samples examined with AFM using NIH-image 1.63 (Fig. 2a). In samples staged at Braak stage 0, a stage at which the brain does not contain NFTs, we detected some, albeit a few, granular tau oligomers. In samples staged at Braak stage I (i.e., neuropathology typically seen in normal brain

Table 1
Demographics and characteristics of cases

Number	Age (years)	Gender	PMT (h:min)	NFT ^a	Senile plaque
1	52	M	15:51	0	0
2	69	F	11:48	0	A
3	82	F	39:04	0	0
4	87	M	70:10	0	0
5	78	M	2:02	0	0
6	66	F	9:51	0	B
7	81	M	3:00	I	B
8	97	F	2:40	I	B
9	84	M	47:25	I	B
10	87	M	4:25	I	C
11	93	M	20:49	I	C
12	86	F	6:50	III	C
13	94	M	13:00	III	C
14	87	F	4:21	III	C
15	82	F	10:32	III	C
16	89	F	16:11	III	C
17	90	F	64:07	V	C
18	86	F	19:51	V	C
19	93	F	13:28	V	C
20	70	M	35:42	V	C
21	80	F	6:41	V	C

Abbreviations: PMT, postmortem time; NFT, neurofibrillary tangle; SP, senile plaque.

^a NFTs and SPs were staged according to the neuropathology staging system of Braak and Braak (1991).

aging), a stage at which entorhinal cortex but not frontal cortex contains NFTs, the number of granular tau oligomers present significantly increased compared to that in the Braak-stage 0 samples ($P = 0.0173$). In samples staged at Braak stage III, a stage at which both limbic areas and entorhinal cortex contain NFTs, the number of granular tau oligomers present also significantly increased compared to that in the Braak-stage 0 samples ($P = 0.0087$). In samples staged at Braak stage V, a stage at which neocortex including frontal cortex contain NFTs, the number of granules increased again significantly compared to that in Braak-stage 0 samples ($P = 0.0087$). We observed no significant differences in the number of granular tau oligomers in stage I, III, and V samples.

We confirmed these results by using Western blotting to assess granular tau oligomer fractions and conventionally purified sarcosyl-insoluble tau fractions derived from Braak-staged frontal cortices (Fig. 2b and c, respectively). The Tau-c immunostaining intensity of tau bands derived from the granular tau oligomer fraction of Braak-stage 0 samples was faint (Fig. 2b). Nonetheless, in Braak-stage I, III, and V samples, we did detect tau smears displaying a immunostaining pattern characteristic of insoluble tau (Fig. 2b cf. PHF-1 immunostaining pattern in Fig. 2c) (Selkoe et al., 1982; Ihara et al., 1983; Greenberg and Davies, 1990). Linear regression analysis revealed a significant correlation between Tau-c immunoreactivity and the number of granular tau oligomers ($P < 0.0001$, $r^2 = 0.6336$). On the other hand, similar statistical analysis failed to reveal a correlation between PHF-1 immunoreactivity and the number of granular tau oligomers.

Taken together, these results indicate that granular tau oligomer levels begin to increase in pre-symptomatic stages of disease, suggesting that granular tau oligomers may form before NFTs are formed.

4. Discussion

4.1. Granular tau oligomer as a pre-symptomatic marker for AD

Using silver-stained human brain sections, Braak and Braak (1991) described seven stages (0–VI) of neuropathology that are now commonly used to stage the progression of neurodegenerative diseases. The Braak staging system is based on the density and distribution of agyrophilic NFTs in the brain (Braak and Braak, 1991). Stage 0 is characterized by the absence of NFTs. Stages I and II are termed transentorhinal stages, because they are characterized by the presence of NFTs in the transentorhinal region. Stages I and II are distinguished by the density of NFTs. Stages III and IV are termed limbic stages, because they are characterized by the presence of NFTs in the hippocampus as well as in the transentorhinal region. Stages V and VI are termed isocortical stages, because they are

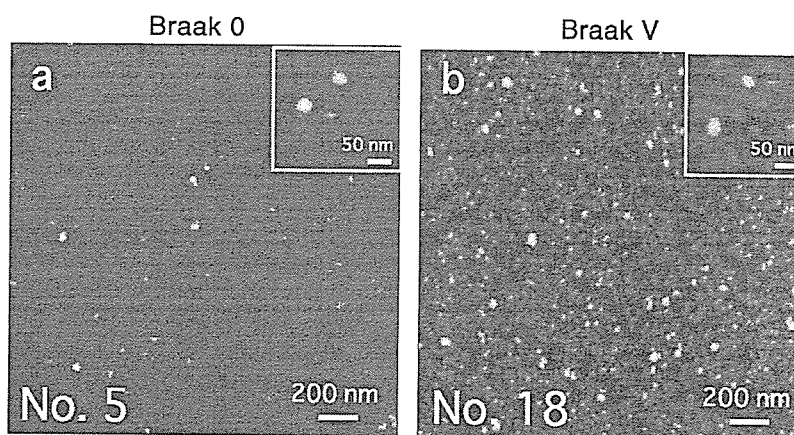


Fig. 1. Granular tau oligomers purified from human frontal cortex. Frontal cortex homogenates were fractionated with sucrose gradient centrifugation, and fractions (fraction 3) containing granular tau oligomers were examined in solution with AFM set to tapping mode. Representative data from the Braak-staged samples indicated are shown here. Insets contain high magnification AFM images of granular tau oligomers. The height range is 30 nm. The large numbers in the lower left corner of each panel correspond to the brain identification numbers in Table 1.

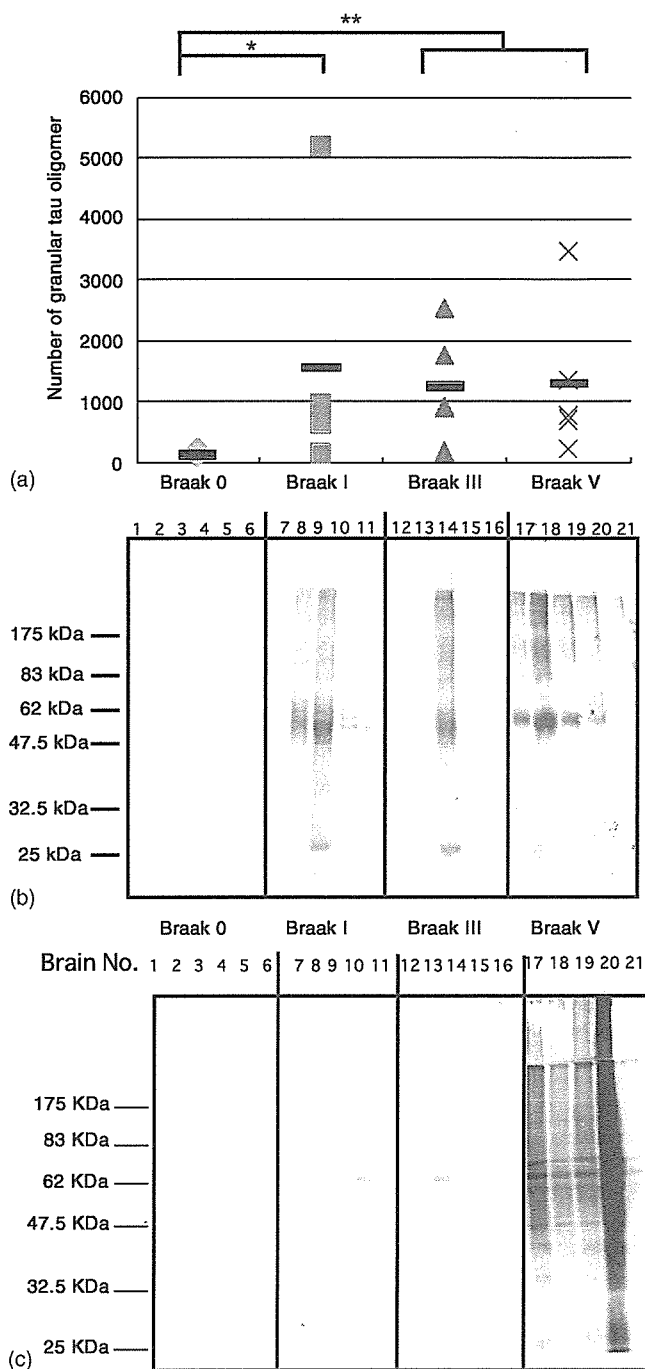


Fig. 2. The distribution of granular tau oligomers observed in different Braak stages. (a) AFM images of Braak-staged frontal cortex samples were analyzed with NIH-image 1.63, and the total number of granular aggregates in each sample were counted and graphed. * $P < 0.05$, ** $P < 0.01$. (b) Western blots of fractions containing granular tau oligomers immunostained with Tau-c antibody. (c) Western blots of sarcosyl-insoluble fractions immunostained with PHF-1 antibody for the detection of tau filaments.

characterized by the extension of NFTs into neocortex, including frontal cortex.

The density and distribution of NFTs have been shown to increase with normal aging (Braak and Braak, 1997). Even non-AD brain specimens from individuals as old as 90 years contain NFTs. In Braak stage I, NFTs are confined within the transentorhinal region. Most of these NFTs are not accompanied

by SPs, suggesting that that NFT formation occurring within the transentorhinal region is independent of SP formation, and thus may not represent a pathological process linked to AD. In line with these data is the finding that the anatomical distribution of NFTs observed in Braak stage I appears to be age dependent (Braak and Braak, 1997), which is consistent with the premise that NFT development occurs as part of normal brain aging.

We detected an increased amount of granular tau oligomers in Braak-stage I frontal cortex samples but not in Braak-stage 0 samples, suggesting that, at a time when NFTs form in the entorhinal cortex, tau dysfunction, which tau comes up from microtubule, and forms aggregate, has already started to occur in the frontal cortex, which should indicate tau dysfunction (Lu and Wood, 1993; Yoshida and Ihara, 1993). Interestingly, the level of granular tau oligomers in frontal cortex remained constant in samples staged at Braak stages II–V, even though the density of NFTs increases progressively in these stages. At this point, however, we cannot explain the incongruity between the levels of tau oligomers and NFTs. We do not know exactly how granular tau oligomers affect neuronal vulnerability.

We also investigated the relationship between granular tau oligomer formation and the density and distribution of senile plaques (SPs) (data not shown), another neuropathological hallmark of AD. We found granular tau oligomers in samples containing SPs in the neocortex (SP-stage B and C). In one Braak-stage 0 sample from an SP-stage B patient (No. 6 in Table 1), however, we did not detect a significant increase in granular tau oligomer levels, suggesting that the extent of SP pathology may not affect the formation of granular tau oligomers. Recently, Katsuno and colleagues reported that the accumulation of A β and tau occurs independently in entorhinal cortex (Katsuno et al., 2005). Therefore, the formation of granular tau oligomers may not be related to A β accumulation but instead may be related to some other aging-related event that occurs during Braak stage I. In later Braak stages, A β may accelerate the formation of granular tau oligomers that ultimately leads to NFT formation and neuronal loss. Further studies are required in order to understand the precise biochemical sequence of events underlying neuronal death, NFT formation, and granular tau oligomer formation.

References

- Braak, H., Braak, E., 1991. Neuropathological staging of Alzheimer-related changes. *Acta Neuropathol. (Berl)* 239–259.
- Braak, H., Braak, E., 1997. Frequency of stages of Alzheimer-related lesions in different age categories. *Neurobiol. Aging* 351–357.
- Gomez-Isla, T., Hollister, R., West, H., Mui, S., Growdon, J.H., Petersen, R.C., Parisi, J.E., Hyman, B.T., 1997. Neuronal loss correlates with but exceeds neurofibrillary tangles in Alzheimer's disease. *Ann. Neurol.* 17–24.
- Greenberg, S.G., Davies, P., 1990. A preparation of Alzheimer paired helical filaments that displays distinct tau proteins by polyacrylamide gel electrophoresis. *Proc. Natl. Acad. Sci. U.S.A.* 5827–5831.
- Hansma, H.G., Laney, D.E., Bezanilla, M., Sinsheimer, R.L., Hansma, P.K., 1995. Applications for atomic force microscopy of DNA. *Biophys. J.* 1672–1677.
- Ihara, Y., 2001. PHF and PHF-like fibrils—cause or consequence? *Neurobiol. Aging* 123–126.
- Ihara, Y., Abraham, C., Selkoe, D.J., 1983. Antibodies to paired helical filaments in Alzheimer's disease do not recognize normal brain proteins. *Nature* 727–730.

- Jicha, G.A., O'Donnell, A., Weaver, C., Angeletti, R., Davies, P., 1999. Hierarchical phosphorylation of recombinant tau by the paired-helical filament-associated protein kinase is dependent on cyclic AMP-dependent protein kinase. *J. Neurochem.* 214–224.
- Katsuno, T., Morishima-Kawashima, M., Saito, Y., Yamanouchi, H., Ishiura, S., Murayama, S., Ihara, Y., 2005. Independent accumulations of tau and amyloid beta-protein in the human entorhinal cortex. *Neurology* 687–692.
- Lee, V.M., Goedert, M., Trojanowski, J.Q., 2001. Neurodegenerative tauopathies. *Annu. Rev. Neurosci.* 1121–1159.
- Lu, Q., Wood, J.G., 1993. Functional studies of Alzheimer's disease tau protein. *J. Neurosci.* 508–515.
- Murayama, S., Saito, Y., 2004. Neuropathological diagnostic criteria for Alzheimer's disease. *Neuropathology* 254–260.
- Reed, L.A., Wszolek, Z.K., Hutton, M., 2001. Phenotypic correlations in FTDP-17. *Neurobiol. Aging* 89–107.
- Saito, Y., Ruberu, N.N., Sawabe, M., Arai, T., Tanaka, N., Kakuta, Y., Yamanouchi, H., Murayama, S., 2004. Staging of argyrophilic grains: an age-associated tauopathy. *J. Neuropathol. Exp. Neurol.* 911–918.
- Santacruz, K., Lewis, J., Spire, T., Paulson, J., Kotilinek, L., Ingelsson, M., Guimaraes, A., DeTure, M., Ramsden, M., McGowan, E., Forster, C., Yue, M., Orne, J., Janus, C., Mariash, A., Kuskowski, M., Hyman, B., Hutton, M., Ashe, K.H., 2005. Tau suppression in a neurodegenerative mouse model improves memory function. *Science* 476–481.
- Selkoe, D.J., Ihara, Y., Salazar, F.J., 1982. Alzheimer's disease: insolubility of partially purified paired helical filaments in sodium dodecyl sulfate and urea. *Science* 1243–1245.
- Takashima, A., Murayama, M., Murayama, O., Kohno, T., Honda, T., Yasutake, K., Nihonmatsu, N., Mercken, M., Yamaguchi, H., Sugihara, S., Wolozin, B., 1998. Presenilin 1 associates with glycogen synthase kinase-3beta and its substrate tau. *Proc. Natl. Acad. Sci. U.S.A.* 9637–9641.
- Tanemura, K., Akagi, T., Murayama, M., Kikuchi, N., Murayama, O., Hashikawa, T., Yoshiike, Y., Park, J.M., Matsuda, K., Nakao, S., Sun, X., Sato, S., Yamaguchi, H., Takashima, A., 2001. Formation of filamentous tau aggregations in transgenic mice expressing V337M human tau. *Neurobiol. Dis.* 1036–1045.
- Tanemura, K., Murayama, M., Akagi, T., Hashikawa, T., Tominaga, T., Ichikawa, M., Yamaguchi, H., Takashima, A., 2002. Neurodegeneration with tau accumulation in a transgenic mouse expressing V337M human tau. *J. Neurosci.* 133–141.
- Tatebayashi, Y., Miyasaka, T., Chui, D.H., Akagi, T., Mishima, K., Iwasaki, K., Fujiwara, M., Tanemura, K., Murayama, M., Ishiguro, K., Planel, E., Sato, S., Hashikawa, T., Takashima, A., 2002. Tau filament formation and associative memory deficit in aged mice expressing mutant (R406W) human tau. *Proc. Natl. Acad. Sci. U.S.A.* 13896–13901.
- von Bergen, M., Barghorn, S., Biernat, J., Mandelkow, E.M., Mandelkow, E., 2005. Tau aggregation is driven by a transition from random coil to beta sheet structure. *Biochim. Biophys. Acta* 158–166.
- Wittmann, C.W., Wszolek, M.F., Shulman, J.M., Salvaterra, P.M., Lewis, J., Hutton, M., Feany, M.B., 2001. Tauopathy in *Drosophila*: neurodegeneration without neurofibrillary tangles. *Science* 711–714.
- Yoshida, H., Ihara, Y., 1993. Tau in paired helical filaments is functionally distinct from fetal tau: assembly incompetence of paired helical filament-tau. *J. Neurochem.* 1183–1186.

Reconstitution of γ -secretase by truncated presenilin (PS) fragments revealed that PS C-terminal transmembrane domain is critical for formation of γ -secretase complex

Hirohisa Shiraishi^{1,2,a}, Toshihiro Marutani¹, Hua-Qin Wang³, Yasuhiro Maeda⁴, Yukihiisa Kurono⁴, Akihiko Takashima⁵, Wataru Araki⁶, Masaki Nishimura³, Katsuhiko Yanagisawa¹ and Hiroto Komano^{1,*}

¹Department of Alzheimer's Disease Research, National Institute for Longevity Sciences, 36-3 Gengo, Morioka, Obu, Aichi 474-8522, Japan

²Organization for Pharmaceutical Safety and Research of Japan, Chiyoda-ku, Tokyo, Japan

³Molecular Neuroscience Research Center, Shiga University of Medical Science, Orsu, Shiga 520-2192, Japan

⁴Faculty of Pharmaceutical Sciences, Nagoya City University, Nagoya, Aichi 467-8603, Japan

⁵Brain Science Institute, RIKEN, Wako, Saitama 350-0198, Japan

⁶Department of Demyelinating Disease and Aging, National Institute of Neuroscience, Tokyo 187-8502, Japan

The presenilin (PS) complex, including PS, nicastrin (NCT), APH-1 and PEN-2, is essential for γ -secretase activity. Previously, the PS C-terminal tail was shown to be essential for γ -secretase activity. Here, to further understand the precise mechanism underlying the activation of γ -secretase regulated by PS cofactors, we focused on the role of the PS1 C-terminal region including transmembrane domain (TM) 8 in γ -secretase activity. For this purpose, we co-expressed C-terminally truncated PS1 (PS1 Δ C) completely lacking γ -secretase activity and the PS1 C-terminal short fragment in PS-null cells, because the successful reconstitution of γ -secretase activity in PS-null cells by the co-expression of PS1 Δ C and the PS1 C-terminal short fragment would allow us to investigate the role of the PS1 C-terminal region in γ -secretase activity. We found that the exogenous expression of the PS1 C-terminal short fragment with NCT and APH-1 completely rescued a defect of the γ -secretase activity of PS1 Δ C in PS-null cells. With this reconstitution system, we demonstrate that both TM8 and the PS1 C-terminal seven-amino-acid-residue tail are involved in the formation of the active γ -secretase complex via the assembly of PS1 with NCT and APH-1.

Introduction

Amyloid β -protein (A β) is the major component of amyloid plaques that are a characteristic feature of the neuropathology of Alzheimer's disease (AD) (Selkoe 2001). Presenilin (PS1 and PS2) is an integral membrane protein that constitutes γ -secretase complex, required for the intramembranous proteolytic cleavage of β -amyloid precursor protein (APP) and the resulting production of A β (for review, see Selkoe 2001). A β has two major C-

terminal variants, the A β that ends at residue 40 (A β 40) and the A β that ends at residue 42 (A β 42). Significantly, all AD-associated mutations in PS genes increase the relative production of A β 42 which is more amyloidogenic than A β 40, although the exact mechanism is not known (for review, see Selkoe 2001).

Recent accumulating evidence has also revealed that PS mediates not only γ -secretase activity (De Strooper *et al.* 1998), but it is also required for several intramembranous cleavages, including the cleavages of notch, CD44, ErbB-4, alcadein (Araki *et al.* 2004) and cadherin (for review, see De Strooper 2003). These results suggest that PS-mediated intramembranous cleavage plays a critical role in several biological functions. PS has a putative eighth transmembrane domain (Li & Greenwald 1998), and full-length PS is endoproteolytically processed into two fragments, the N-terminal fragment (NTF) and

Communicated by: Yoshinori Ohsumi

*Correspondence: E-mail: hkomano@nils.go.jp

^aPresent address: Department of Physiology & Biophysics, Zilkha Neurogenetic Institute, Keck School of Medicine, University of Southern California, Los Angeles, CA 90033, USA.

DOI: 10.1111/j.1365-2443.2005.00914.x

© 2005 The Author(s)

Journal compilation © 2005 by the Molecular Biology Society of Japan/Blackwell Publishing Ltd.

Genes to Cells (2006) 11, 83–93

83

the C-terminal fragment (CTF) between transmembrane domain (TM) 6 and TM7 (Thinakaran *et al.* 1996). The cellular level of processed PS is tightly limited (Ratovitski *et al.* 1997; Thinakaran *et al.* 1997), and the processed PS resides in a high-molecular-weight complex that includes mature glycosylated NCT, APH-1 and PEN-2 (for review, see De Strooper 2003). Several lines of evidence clearly established that NCT, APH-1 and PEN-2 (collectively named PS cofactors in this study) are required for PS endoproteolysis and the formation of the active γ -secretase complex (Francis *et al.* 2002; Edbauer *et al.* 2003; Kimberly *et al.* 2003; Takasugi *et al.* 2003). However, it remains to be elucidated how PS cofactors regulate γ -secretase activity and PS endoproteolysis.

PS contains two conserved, essential aspartate residues in adjacent TM6 and TM7 that may define a novel aspartyl protease active site (Wolfe *et al.* 1999; Steiner *et al.* 2000; Li *et al.* 2000b; Weihofen *et al.* 2002). However, the precise catalytic mechanism underlying the formation of the γ -secretase complex, including the roles of TMs and PS cofactors in γ -secretase activity, is not completely understood. Previously, it was shown that a short C-terminal tail of PS is required for PS endoproteolysis and/or γ -secretase activity (Tomita *et al.* 1999; Shirotani *et al.* 2000). Here, to gain deep insights into the mechanism underlying the formation of active γ -secretase, we focused on the role of the PS1 C-terminal region including TM8 in γ -secretase activity. For this purpose, we co-expressed C-terminally truncated PS1 (PS1 Δ C) completely lacking γ -secretase activity and the PS1 C-terminal short fragment in PS-null cells. Previously, it was shown that the co-expression of PS1 NTF and CTF restored γ -secretase activity in PS-null cells (Laudon *et al.* 2004; Shiraishi *et al.* 2004). However, it was not known whether the exogenous expression of PS1 C-terminal short fragment can rescue a defect in the γ -secretase activity of PS1 Δ C. In this study, we found that the exogenous expression of the PS1 C-terminal short fragment with NCT and APH-1 completely rescued a defect of the γ -secretase activity of PS1 Δ C in PS-null cells. With this reconstitution system, we demonstrate that both TM8 and the PS1 C-terminal seven-amino-acid-residue tail are involved in the formation of the active γ -secretase complex via the assembly of PS1 with NCT and APH-1.

Results

To clarify the role of the PS1 C-terminal region including C-terminal TM8 in γ -secretase activity, we constructed C-terminally truncated PS1 (PS1 Δ C) and the

PS1 C-terminal short fragment. As shown in Fig. 1A, PS1 Δ C66 lacks PS1 C-terminal 66 amino acid residues including TM8, and PS1 Δ C37, which was truncated downstream of TM8, lacks C-terminal 37 amino acid residues including the PALP sequence (Tomita *et al.* 2001). We also constructed cDNA encoding the PS1 C-terminal short fragment starting at methionine. C68 and C37 correspond to the fragments of the first methionine plus PS1 C-terminal 68 and 37 amino acid residues, respectively. PS1 Δ C66 and PS1 Δ C37 exhibited the complete loss of A β generation and PS endoproteolysis in PS-null cells, as observed in the PS1 mutant with other short C-terminal truncations (Bergman *et al.* 2004) (Fig. 1B).

We first investigated whether the co-expression of PS1 Δ C66 and PS1 cofactors restore A β generation in PS-null cells (Fig. 2A, left 5 lanes). As shown in Fig. 2A (lanes 1–5), no A β generation was observed, suggesting that PS1 Δ C66 failed to form the active γ -secretase complex with PS cofactors. However, the exogenous expression of C68 with the APH-1b and NCT completely rescued a defect in the γ -secretase activity of PS1 Δ C66, although the expression of C68 without PS cofactors did not affect γ -secretase activity (Fig. 2A, lanes 6–8). The endogenous level of PEN-2 was found to be slightly increased in the co-expression of PS1 Δ C66, C68, APH-1b and NCT, but the endogenous level of PEN-2 was not as high as that of PS null cells expressing full-length PS (Fig. 2B). Therefore, the exogenous expression of PEN-2 was expected to further enhance the reconstituted γ -secretase activity. However, a further increase in γ -secretase activity was not observed when PEN-2 was additionally co-expressed with C68, APH-1b and NCT (Fig. 2A, lane 9). The limiting factors for γ -secretase activity in this reconstitution system were found to be both APH-1 and NCT as shown in Fig. 2C. The rescue in a defect in PS1 Δ C66 endoproteolysis was also observed by the co-expression of C68, APH-1b and NCT (Fig. 2A, lane 8), and PS1 Δ C66 endoproteolysis was further stimulated by the expression of PEN-2 with C68, APH-1b and NCT (Fig. 2A, lane 9). Previously, the C-terminal short tail of PS was shown to be required for PS endoproteolysis and PS stabilization (Tomita *et al.* 1999; Shirotani *et al.* 2000). Therefore, we next investigated whether the expression of C68 lacking the last seven amino acid residues (C68 Δ C7) with PS cofactors also rescues the defects in γ -secretase activity and PS1 Δ C66 endoproteolysis. The result showed that the co-expression of C68 Δ C7 and PS cofactors did not restore γ -secretase activity and endoproteolysis (Fig. 2A, lanes 10 and 11), indicating that the rescue by the co-expression of C68 and PS cofactors is completely dependent on the presence of

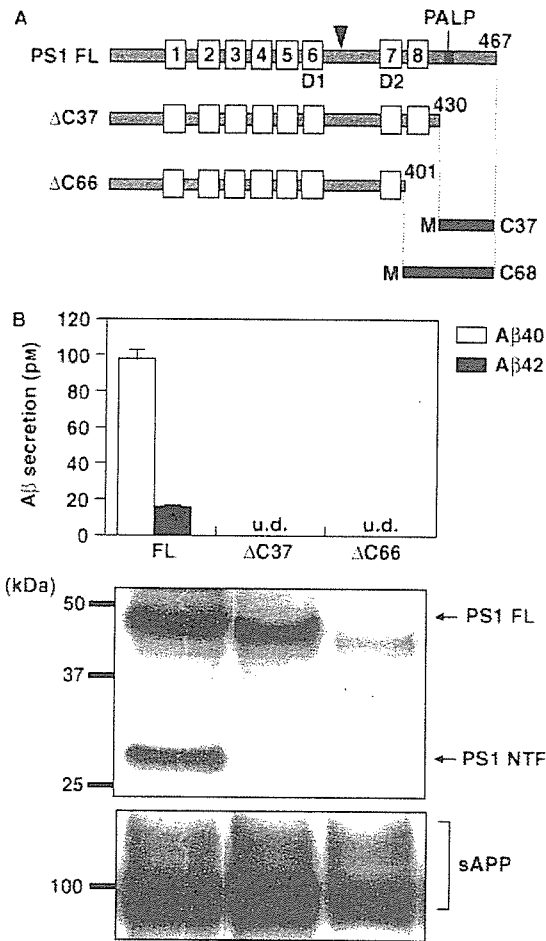


Figure 1 Schematic diagram of C-terminally truncated forms of PS1 (PS1ΔC) and PS1 C-terminal fragments expressed in (A) PS-null cells, and (B) a defect in Aβ generation and endoproteolysis of PS1ΔC. (A) A schematic diagram of C-terminally truncated forms of PS1 used in this study is shown. The last 37 (ΔC37) or 66 (ΔC66) amino acid residues of PS1 were deleted. PS1 C-terminal fragments starting at Met (M) encoded by the cDNAs used in this study are also shown. C37, Met plus the PS1 C-terminal 37 amino acid residues; C68, Met plus the PS1 C-terminal 68 amino acid residues. Boxes with numbers illustrate putative transmembrane domains (TM). D1 and D2, two aspartates essential for γ-secretase activity; PALP, the PALP sequence (56); FL, full-length; arrowhead, the site of endoproteolytic processing; number denotes the position of an amino acid residue at the C-terminus. (B) APP695 and the full-length (FL) PS1 or PS1ΔC were retrovirally expressed in PS-null cells (2×10^5); Aβ40 and Aβ42 secreted from cells during a 48-h culture were quantified by ELISA (the upper panel). u.d., Aβ was not detected (< 10 pM). Values are means \pm SD of two independent dishes ($n = 2$). CHAPSO-solubilized lysates (10 μg) were immunoblotted with the anti-PS1 NTF antibody (the middle panel). Soluble APP secreted from cells were immunoblotted with the anti-APP antibody, 22C11 (the bottom panel).

the C-terminal seven-amino-acid-residue tail (Fig. 2, lanes 10 and 11). It was also noted that the extent of Aβ generation from the reconstituted γ-secretase induced by the co-expression of PS1ΔC66, C68 and PS cofactors was higher than that from the co-expression of PS1 FL and PS cofactors.

To further investigate the effects of the co-expression of PS1ΔC66 and C68 on the assembly of the active γ-secretase complex, we performed the co-immunoprecipitation experiment using an anti-PS1 NTF antibody (Fig. 3). As shown in Fig. 3A, APH-1b and NCT failed to co-immunoprecipitate with PS1ΔC66 (Fig. 3A, lanes 1–4), but they were co-immunoprecipitated when C68 was co-expressed (Fig. 3A, lanes 5 and 6); however, PEN-2 co-immunoprecipitated with PS1ΔC66 even when exogenous C68 was not expressed (Fig. 3, lanes 4 and 6). It is also noted that the level of mature NCT in the complex reconstituted with PS1ΔC66 and C68 was lower than that when PS1 FL with cofactors are expressed (Fig. 3, lanes 1 and 2; lanes 5 and 6). We also confirmed that C68 has the domain(s) for the binding of NCT and APH-1 by co-immunoprecipitation in the cells expressing C68 in the absence of the PS1ΔC66 (Supplementary Fig. S1).

In addition, when C68ΔC7 was expressed, no assembly of PS1ΔC66 with PS cofactors was observed (Fig. 3A, lanes 7 and 8). We also found that the level of C68ΔC7 bound to PS1ΔC66 was lower than that of C68 bound to PS1ΔC66 (Fig. 3A, bottom panel). The co-immunoprecipitation experiment using the anti-NCT antibody also demonstrated that the smaller amount of C68ΔC7 co-immunoprecipitates with NCT than that of C68 (Fig. 3B). This result indicates that the assembly of C68, not only with PS1ΔC66, but also with NCT, requires the presence of the C-terminal seven-amino-acid-residue tail. This result agrees with a result of a recent study showing that PS1 C-terminus binds to NCT (Kaether *et al.* 2004). Taken together, the rescue of the defects in γ-secretase activity and PS1ΔC66 endoproteolysis by the expression of C68 with PS cofactors is accompanied by the rescue of a defect in the assembly of PS1ΔC66 with APH-1b and NCT.

We next determined the role of TM8 in γ-secretase activity with this reconstitution system of γ-secretase activity. For this purpose, we co-expressed PS1ΔC66 and C37 that lacks TM8 in PS-null cells (Figs 1A and 4A). As shown in Fig. 4A, the co-expression of C37 and PS cofactors did not rescue the defects in γ-secretase activity and PS1ΔC66 endoproteolysis. This result suggests that the TM8 region of C68 is necessary for the functional rescue of inactive PS1ΔC66. However, we cannot exclude the possibility that C37 does not have an ability to rescue

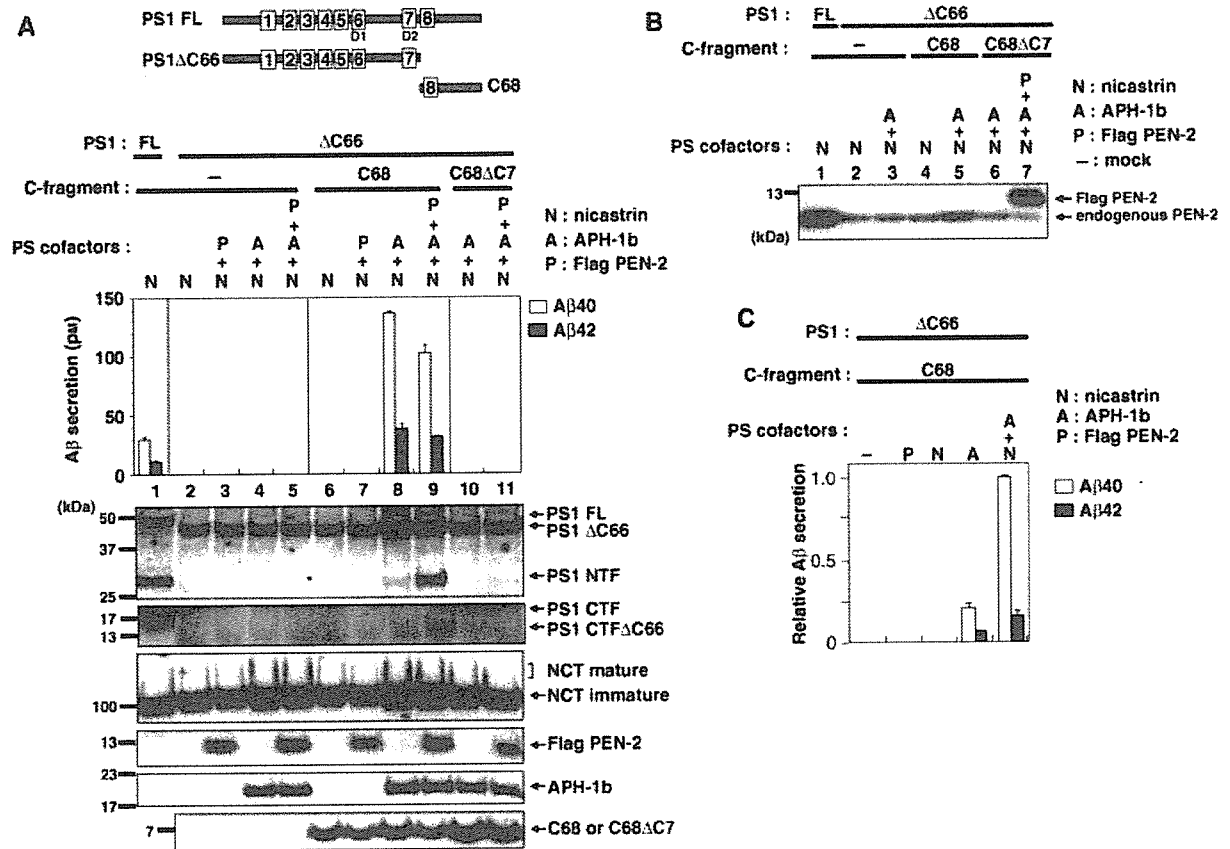


Figure 2 The expression of C68 with PS cofactors rescued defects in γ -secretase activity and endoproteolysis of PS1 Δ C66. (A) After APP695 and the indicated exogenous PS cofactors were retrovirally expressed with PS1 Δ C66 and C68 or C68 Δ C7 in PS-null cells, A β secreted from these cells during a 48-h culture was quantified by ELISA, and CHAPSO-solubilized lysate (10 μ g) was immunoblotted with the anti-PS1 NTF antibody (for the detection of PS1 FL, PS1 Δ C66 and PS1 NTF), anti-PS1 loop monoclonal antibody (for the detection of PS1 CTF and CTF Δ C66), anti-APH-1b antibody, anti-FLAG antibody (for the detection of PEN-2), anti-NCT antibody and the anti-PS1C-20 antibody (for the detection of C68 or C68 Δ C7). C-fragment, C-terminal short fragment; -, mock transfection (pMX). Values are means \pm SD of two independent dishes ($n = 2$). Data are representative of three independent experiments. (B) The same lysates prepared from the PS-null cells retrovirally expressing the indicated truncated PS and PS cofactors as described in Figure 2A were immunoblotted with anti-PEN-2 antibody for the detection of endogenous PEN-2. (C) After APP695 and the indicated exogenous PS cofactors (-, mock transfection) were retrovirally expressed with PS1 Δ C66 in PS-null cells, A β secreted from these cells during a 48-h culture was quantified by ELISA. The A β levels were expressed as relative to A β 40 levels obtained from PS-null cells expressing PS1 Δ C66 with NCT and APH-1b.

a defect in γ -secretase activity. Therefore, we next determined whether C37 has an ability to rescue inactive PS1 Δ C, or whether TM8 is necessary for the functional rescue of inactive PS1 Δ C in PS-null cells. For this purpose, we investigated whether the co-expression of C37 and PS1 Δ C37 truncated downstream of TM8 (Figs 1A and 4B) restores γ -secretase activity in PS-null cells. As shown in Fig. 4B, the defects in γ -secretase activity and PS1 Δ C37 endoproteolysis were completely rescued by the expression of C37 with APH-1b and NCT, although they were not rescued by the expression of exogenous PS

cofactors without C37 (Fig. 4B, lanes 2–9). These results indicate that TM8 is necessary for the rescue of γ -secretase activity and PS1 endoproteolysis by the co-expression of PS1 Δ C and the PS1 C-terminal fragment with PS cofactors in PS-null cells. The rescue by the co-expression of C37 and PS cofactors was also completely dependent on the presence of the C-terminal seven-amino-acid-residue tail (Fig. 4, lanes 10 and 11). It is also noted that the level of C37 is higher when APH-1 and NCT were co-expressed, compared with that when APH-1 was not expressed (Fig. 4A, lanes 2–5 and Fig. 4B, lanes 6–9).